بسم الله الرحمن الرحيم

Sudan University of Science and Technology
College of Post Graduate Studies

دراسة الخصائص التركيبية والضوئية لأغشية النيكل المشوبة بالألمونيوم والكبريت وتطبيقاتها علي الخلايا الشمسية

A Study of the Structural and Optical Properties of Nickel Doped Aluminum and Sulfur Films and its Application on Solar Cells

Thesis Submitted for the Degree "Doctor of Philosophy"

Submitted by

Mohamed Hamdan Hussen Ahmed

Supervision by

Rawia Abdelgani Elobaid

Co- supervision associated

Professor Mubarak Dirar Abdullah

December 2022

الآيـــــة

بسم الله الرحمن الرحيم

قَالَ تَعَالَىٰ:

﴿ ٱللَّهُ لَآ إِلَٰهَ إِلَّا هُوَ ٱلۡحَيُّ ٱلۡقَيُّومُۚ لَا تَأۡخُذُهُۥ سِنَةٞ وَلَا نَوۡمٞۚ لَّهُۥ مَا فِي ٱلسَّمَٰوَٰتِ وَمَا فِي ٱلۡأَرۡضِۗ مَن ذَا ٱلَّذِي يَشۡفَعُ عِندَهُۥٓ إِلَّا بِإِذۡنِهِۦۚ يَعۡلَمُ مَا بَيۡنَ أَيۡدِيهِمۡ وَمَا خَلۡفَهُمۡۖ وَلَا يُحِيطُونَ بِشَيۡءٖ مِّنۡ عِلۡمِهِۦٓ إِلَّا بِمَا شَآءَۚ وَسِعَ كُرۡسِيُّهُ ٱلسَّمَٰوَٰتِ وَٱلۡأَرۡضَۖ وَلَا يَـُٔودُهُۥ حِفۡظُهُمَاۚ وَهُوَ ٱلۡعَلِيُّ ٱلۡعَظِيمُ ٢٥٥ ﴾

صدق الله العظيم

سورة البقرة: ـ الآية (٢٥٥)

Dedication

To those enlightened my way, urged me to succeed and encouraged me reach the highest goal.

To my parents

I dedicate this thesis to my:

mother and father,

my dear sisters and brothers,

to my wife, and my daughter Shiraz

and every person who helped me to finish this work.

To my teachers and friends

Acknowledgment

Firstly, my praise to Allah Whom blessed me with good health to complete this work.

I wish to express my sincere thanks and appreciation to my supervisor Prof. **Mubark Dirar Abdullah** and for his supervision **Rawia Abdelgani Elobaid** and valuable guidance during the research period, his sincere technical advice and support that allowed me to complete this work.

I have to express my gratitude to the laboratories of Al-Neenlen University Abd Elsakhi.

Thank also extend to department of physics, science college, graduate study college and Sudan university of science and technology

Abstract

Five samples of Ni_x AL $_{2(1-x)}$ and five other samples of $Ni_xS_{1-x}O_4$ were prepared to be used as solar cell. The aim of this work is to characterize these films to see how there can used as solar cells.

The crystal and Nano structure has been characterized by using X-ray diffraction technique. The optical and electrical properties where characterized using ultraviolet spectrometer. The performance as a solar cell was tested using simple electric circuit. The result for $Ni_xAL_{2(1-x)}$ indicates that increasing Ni concentration X increase the energy gap while the Nano crystal size, d-spacing, mass density, absorption coefficient and solar cell efficiency decrease. For $Ni_xS_{1-x}O_4$ the result obtains shoes that increasing Ni concentration increases the Nano crystal size, crystal spacing, absorption coefficient and efficiency.

المستخلص

حضرت خمس عينات من النيكل المطعم بـالألمونيوم و خمس عينـات أخـري من النيكل المطعم بالكبريت لاستخدامها كخلايا شمسية. لذا يهدف هذا البحث لتوصيف هذه الشرائح الرقيقة لمعرفة كيفية إستخدامها. أستخدمت تقنية حيود الأشعة السينية لمعرفة التركيب البلوري والنانوي. أما الخواص الضوئية والكهربية فتم توصيفها باستخدام المطياف فوق البنفسجي. تم اختبار الأداء كخلية شمسية باستخدام دائرة كهربية بسيطة.بينت نتيجة النيكل المطعم بـالألمونيوم أن زيادة تركيز النيكل يزيد فجوة الطاقة، في حين ينقص الحجم النانوي البلوري والمسافة بين المستويات البلورية وتنقص كذلك كثافة الكتلة ومعامل الامتصاص وكفاءة الخلية الشمسية.أما بالنسبة للنيكل المطعم بالكبريت فإن النتائج أوضحت ان زيادة تركيز النيكل تزيد الحجم البلوري النانوي والمسافة بين المستويات البلورية ومعامل الامتصاص والكفاءة.

List of Contents

List of Table

List of Figures

Chapter One

Introduction

(1.1) Energy and life

The electricity demand in the world's developing countries is increasing rapidly and it is a great challenge to meet this demand, without affecting the climate and the environment. The main energy source for power production in the world today is fossil fuels. However, with threatening climate change the use of these must arguably decrease. The power generation is globally the largest source of green-house gases and, preferably, the generation should be shifted to more renewable sources. There are a lot of alternatives to fossil fuels, but the cost is in most cases higher than for conversion of fossil fuels. Solar power is often regarded as one of the most promising energy sources for the future. Solar energy can be used in a number of ways. For electricity generation the most common process is through solar photovoltaic. Solar PV cells have long been used to power small electronic devices such as calculators. But large groups of solar PV cells can be added together, powering small solar panels in individual households or larger arrays feeding power directly into the electricity grid. [1] Energy is important for human life it is used in wide variety of applications food cooking, operation of electronic devices and light need heat and electrical energy transportation systems beside telecommunication system also need energy the most wide spreader energy source is the electric and petroleum energy unfortunately the electric and petroleum energy are expensive and causes environmental pollution thus one need cheap and non-pollutant energy pollutant energy source.

(1.2) Research Problem

The energy currently used causes environmental pollution and combustion on the globe , so there must be clean energy which is the solar cells but the problem of solar cell is there low efficiency , high cost , and complicated manufacture therefore , we use Nano since to obtain solar cells at an urgent cost and high efficiency

(1.3)Aim of the Work

The objectives of the present research can be summarized as follows:

1- Characterize the crystals structure and pure phase by using XRD diffraction patterns.

2- Characterize the surface morphology of the ATO nanoparticles by Scanning Electron Microscopy. $Ni_x Al_{2(x-1)}O_4$ and $Ni_x S_{1-x} O_4$

3- Application of some Nano structured thin film. $Ni_x Al_{2(x-1)}O_4$ and $Ni_x S_{1-x} O_4$ to dye-sensitized solar cell

(1.4) Research Methodology

1. 1-prepare 5 samples from Ni_x doped $Al_{2(x-1)}O_4$ having different Nano size.
2. 2-prepare 5 samples from Ni_x doped $S_{1-x} O_4$ having different Nano size.
3. Determination of optical properties using UV-visible absorption spectrophotometer.
4. Determination of The structure of the samples was characterized by X-ray diffraction (XRD).
5. Determination of the FTIR spectroscopy is a investigating materials. It is based on the interaction electromagnetic radiation and natural vibration of chemical bonds among atoms that compose the matter.
6. Compare result with previous studies.

(1-5) Thesis Layout

1. 1st year : literature Review
2. 2nd year :Experimental work
3. 3^{rd} year :Writing

Chapter Two

Theoretical Background

(2.1) Solar energy and electric power production

At present, the total energy consumption in the world is fourteen tera-watts (TW) at any given moment, and this consumption is estimated to be about two times higher by2050 To meet this demand, all forms of energy need to be increased rapidly in the coming years. The use of traditional energy resources such as fossils fuel is not justifiable, due to its pollution and greenhouse gas emissions. Solar energy is available in abundance in most parts of the world. The amount of solar energy incident on the earth's surface is approximately1.5 x 10^{18} kWh/year, which is about 10,000 times the current annual energy consumption of the entire world. The density of power radiated from the sun (referred to as solar energy constant) is 1.373 kW/m2. [2] For this reason, there has been rapid development of renewable energy technologies to meet the future energy demand and creates a sustainable free pollution energy economy.

Among the various ways of harvesting energy from Mother Nature, solar energy has become one of the dominant forms due to its availability. According to recent data, the annual energy reaching the earth's surface from the sun is larger than all forms of traditional energy resources that have ever been available, or will ever be available, from all of the non-renewable sources on the earth including oil, coal, natural gas, and nuclear power [3]

Solar energy currently provides only a quarter of a percent of the planet electricity supply; however, this industry is growing at a staggering speed as photovoltaic (PV) panels have the advantage of being almost maintenance and pollution free.

Another way to generate electricity from solar energy is to use photovoltaic cells, magic slivers of silicon that converts the solar energy falling on them directly into electricity. Large scale applications of photovoltaic for power generation, either on the rooftops of houses or in large fields connected to the utility grid are promising as well to provide clean, safe and strategically sound alternatives to current methods of electricity generation

(2.2) Semiconductor materials

Semiconductors are considered as the heart of modern day consumer, industrial and research electronics. These materials have the electrical conductivity ranging in between the conductors (Cu, Au, etc.) and insulators (glass, wood etc.). As a consequence, a semiconductor can have a number of distinct properties. Among these, the most important one is the variation in its conductivity by incorporating impurities (doping) or by exposing to external disturbances such as electric field or electromagnetic radiation (light and/or ionizing radiation, etc). Such ability of tuning electric characteristics make these materials very useful for functional devices that can amplify, act as a switch, or convert optical energy to electrical energy. Semiconductors have been classified into groups by many different ways. Semiconductors can be elemental or compound as described Another way of distinguishing semiconductors is from their energy band gaps. For example, depending on the electronic energy band gap, these can be divided into two groups namely narrow and wide band gap semiconductors. Narrow band gap semiconductors have electronic band gap comparatively smaller than Si (1.1 eV). e.g., InSb (0.17eV), InAs (0.354 eV) and PbTe (0.32 eV), etc., at room temperature . The narrow band gap semiconductors are also used for fabricating infrared detectors, etc. Conversely, the semiconductors with electronic band gap larger than that of Si or 2.0 eV are considered as wide band gap semiconductors, e.g., TiO2 (3.0 - 3.25) eV, ZnO (3.3 eV) and ZnS (3.54 - 3.91) eV.[4]

(2.2 -1) Semiconductor materials in photocatalysis

Semiconductor materials are crystalline solids with electrical conductivity between conductors (metals) and insulators, in which the electric charge carrier density can be changed by external means. In a semiconductor, the electrical resistance decreases as temperature increases, which is the opposite behavior in metal. In Figure 2-8 it is shown the energetic band structure for the conductive, semiconductor, and insulator materials.

Semiconductors materials can display a range of useful properties such as current can pass easily, variable resistance, and sensitivity to light or heat . Since their electric properties can be modified by doping or by application of an external electrical field or light, devices containing semiconductors can be used for amplification, switching, and energy conversion [5]

Practical applications of the semiconductors include laser diodes, electronic devices, solar cells, microwave-frequency integrated circuits, and photocatalysis.

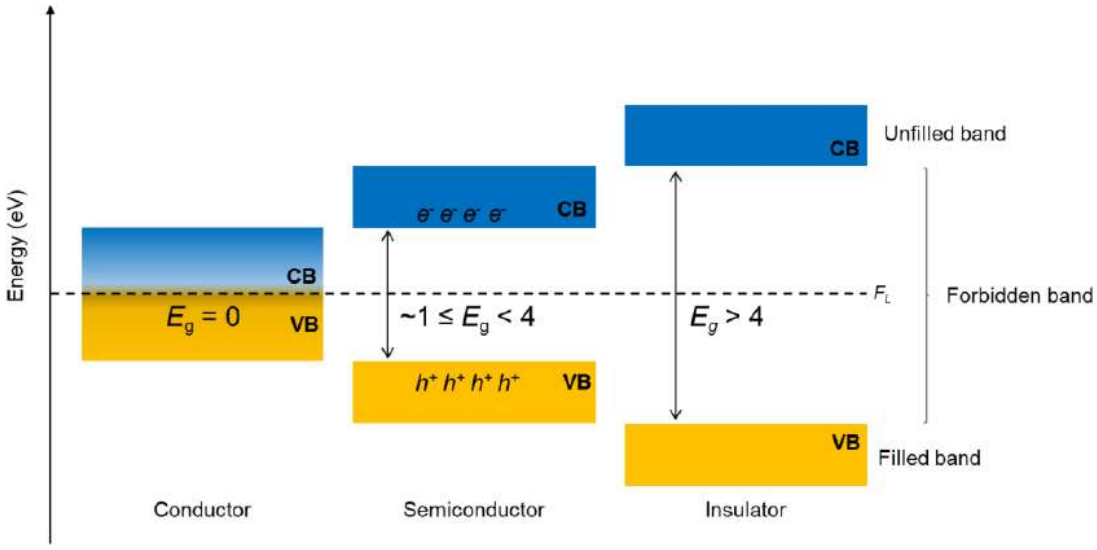

Figure (2-1) Band structure energy for conductive, semiconductor and insulator materials.

In a solid semiconductor, the band of higher energy filled with electrons is the VB, and the band with the lowest unfilled energy is the CB. The range energies between VB and CB are defined as a forbidden band and delimits in which electrons are not allowed to transit [6]**.**

The range of *E*g allows distinguishing conductive materials from semiconductor and insulator materials (Figure 2-1). In conductive materials, the VB overlaps with the CB (*E*g = 0 eV). Therefore, there is a high density of electrons that contribute to the high electrical conductivity that characterizes these materials. For semiconductor and insulator materials, the *E*g > 0 eV, with the bandgap energy being substantially higher for isolating materials, typically *E*g > 4 eV. The semiconductors can be activated either by thermal excitation or by absorption of radiation energy equal or higher than *Eg* (E ≥ *E*g), giving rise to excited states, as illustrated**.** The band structure of a crystalline semiconductor material can be described by the relationship between energy *E* and the *k*-vector**.** Thus, the minimum energy states of the conduction band and the maximum energy of the valence band are characterized by an energy value and a *k*-vector. In a direct bandgap semiconductor, the maximum VB and the minimum CB occur for the same *k*-vector (Δ*k* = 0). In this case, the transition between two levels is

allowed and corresponds to bandgap energy, so the electron of VB is transferred to CB with the same momentum. Therefore, no momentum transfer is required to launch the electron from the VB into the CB [7]**.**

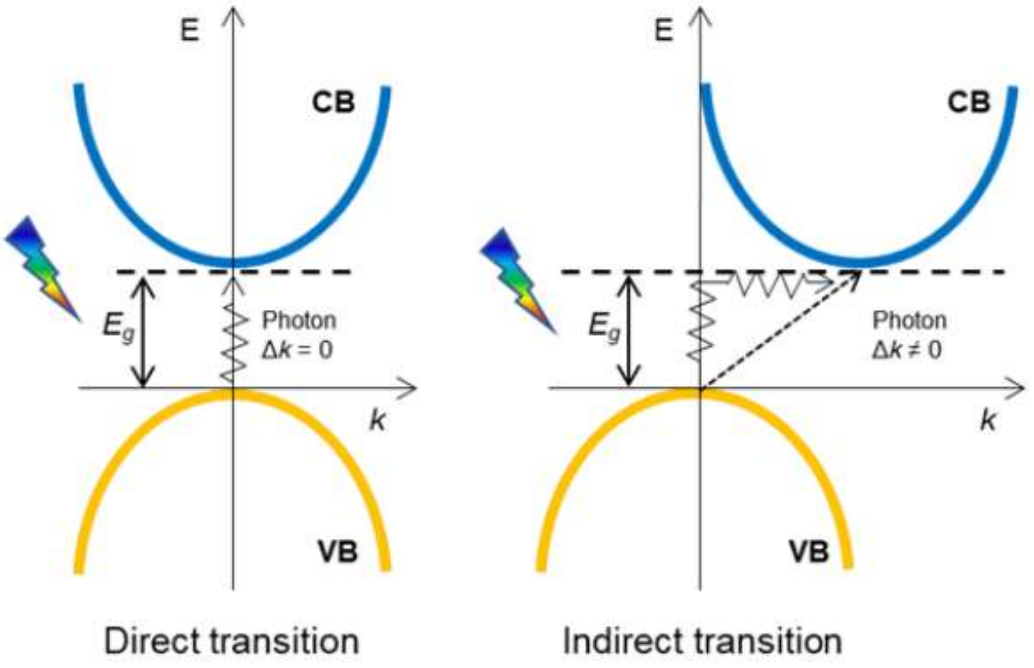

Figure (2-2) Schematic representation of the excitation process in semiconductor materials, from the top of the valence band to the bottom of the conduction band, by photonic absorption, following a direct and an indirect transition process

In an indirect bandgap semiconductor, the maximum VB and the minimum CB occur for different *k*-vector, and thus it is given without conservation of linear momentum since *k* is changed ($\Delta k \neq 0$). Therefore, a fast electron has to transfer momentum to an electron in VB in order to excite it into the conduction band. This also implies that the cross-section for interband transitions is lower than in the case of direct semiconductors [8, 9].

If semiconductors materials are aimed for photocatalysis, they can be modified by different approaches, including doping, synergetic combination with other semiconductors (formation of composites), or surface sensitization [10,11,12]**.** This can open the possibility to control the properties of the semiconductors, for instance, by introduction levels in the forbidden zone, which can decrease the *e*-/*h*+ recombination.

This intermediate energy level can also act as either an electron acceptor or a donor, which allows the semiconductor to absorb visible light [11]**.** For example, wide bandgap semiconductors (such as ZnO and TiO2) can be photoactivated by visible illumination, after

defect engineering or doping. Defect engineering involves the controlled introduction of native defects, such as vacancies or interstitials, while doping implies the controlled incorporation of impurities into the crystal lattice [13]

Doping can be achieved, during semiconductor synthesis using a trace element (*e.g.*, metal) or a chemical doping agent (*e.g*., non-metal). The dopant will be incorporated into the crystalline structure, to give the material different electrical properties than the pure semiconductor. Doping with metals can introduce extra levels in the forbidden band (as mention above), and doping with non-metal, such as N, F, C, or P, can extend the light absorption of the semiconductor into the visible region [11].

For instance, anion doping could affect the TiO2 conduction band, which has the contribution of Ti 3*d*, 4*s*, and 4*p* orbitals. In this case, the anion doping usually changes the valence band position and shifts it upward to narrow the bandgap of TiO2. For example, N is the most suitable doping element as its *p* orbitals could contribute to shifting the VB due to the synergic action with the O 2*p* orbitals, which can narrow the bandgap of TiO2 by shifting the VB upward [11].

There are two types of intrinsic semiconductors materials, *n*-type and *p*-type. The semiconductor type depends on the position of the Fermi level (*FL*). If the *FL* is near to the conduction band, it is an *n*-type semiconductor. On the other hand, *p*-type is a semiconductor with the Fermi level close to the valence band. For example, TiO2 displays *n*-type semiconducting properties due to a tendency for oxygen deficiency which manifests itself in the formation of either oxygen vacancies or titanium interstitials; both are donor-type defects [14].

ZnO is also an *n*-type semiconductor, due to the majority of carriers on this material are electrons. However, NiO is a *p*-type semiconductor once have holes as the majority carriers. For instance, Cu2O for example is an intrinsic *p*-type semiconductor [15].

However, the type of intrinsic semiconductors materials can be changed by doping, forming extrinsic semiconductors. Semiconductors can be *n*- or *p*doped (Figure 2-10). *n*-Type semiconductors are created by doping an intrinsic semiconductor with an electron donor element (*n*- comes from the negative charge of the electron). Here, the electrons are the majority carriers, and holes are the minority ones. In this case, the Fermi level (*FL*) is higher than that of the intrinsic semiconductor and lies closer to the conduction band than the valence band, as depicted in Figure 2-10. *p*-Type semiconductors can be formed by doping with an electron acceptor element (*p*- refers to the positive charge of a hole). In opposition to*n*-type semiconductors, the *p*-

type has a larger hole concentration, which is the majority charge carriers. For *p*-type semiconductors, the *FL* is below the intrinsic *FL* and lies closer to the valence band than the conduction band, as shown in Figure 2.3.

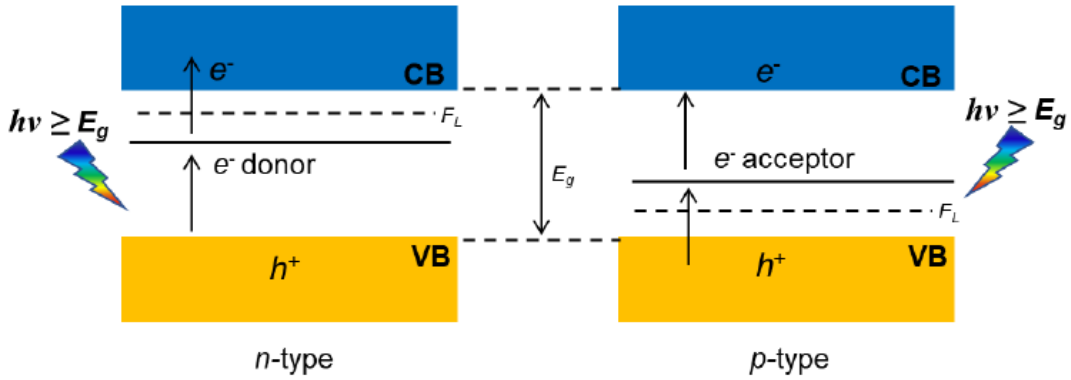

Figure (2-3) Representation of *n*- and *p*-type doping in a semiconductor.

Several semiconductors including TiO2, ZnO, CdS, WO3, ZrTiO4, SnO2, CeO2 and CuO, have been used, for photo(electro)catalysis [16-17].

Recently other semiconductor materials with improved photocatalytic response have been reported, such as carbon nanotubes (CNT**)** [18],

titanate elongated nanoparticles (TNP) [19,20] transition metal sulphides (*i.e.* Bi2S3, ZnS and Ag2S) [19,21]**,** spinels, perovskites, zeolites or activated carbon [22]**.** In addition, the synergetic combination of two or more components, for example in TiO2/Ag2CrO4, [23] ZnO/Ag/Ag2WO4 or Fe3O4/ZnO/CoWO4 [24], it allows the enhancement of photocatalytic properties due to the absorption improvement in the visible range and also the decrease on the charge carriers recombination. For instance, in order to have active photocatalytic materials under visible light, a proficient way to extend the absorbance of TiO2 to visible light can be the development of heterojunctions of different semiconductors. These semiconductor combinations, such as Fe2O3/TiO2, TiO2/SnO2, ZnO/TiO2, and WO3/TiO2, have been shown synergetic photocatalytic effects when used for pollutants degradation [25]

(2.3) Photovoltaic energy

Photovoltaic (PV) is a method of generating electrical power by converting solar radiation into direct current electricity using semiconductors that exhibit the photovoltaic effect. Photovoltaic is the field of technology and research related to the devices which directly convert sunlight into electricity. The solar cell is the elementary building block of the photovoltaic technology. Solar cells are made of semiconductor materials, such as silicon. One of the properties of semiconductors that makes them most useful is that their conductivity may easily be modified by introducing impurities into their crystal lattice. [26] Photovoltaic offer consumers the ability to generate electricity in a clean, quiet and reliable way. Photovoltaic systems are comprised of photovoltaic cells, devices that convert light energy directly into electricity. It is anticipated that photovoltaic systems will experience an enormous increase in the decades to come. However, a successful integration of solar energy technologies into the existing energy structure depends also on a detailed knowledge of the solar resource. But to note it is 2.4essential to state the amount of literature on solar energy, the solar energy system and grid connected system is enormous. Grid interconnection of photovoltaic (PV) power generation system has the advantage of more effective utilization of generated power. However, the technical requirements from both the utility power system grid side and the PV system side need to be satisfied to ensure the safety of the PV installer and the reliability of the utility grid. [27]

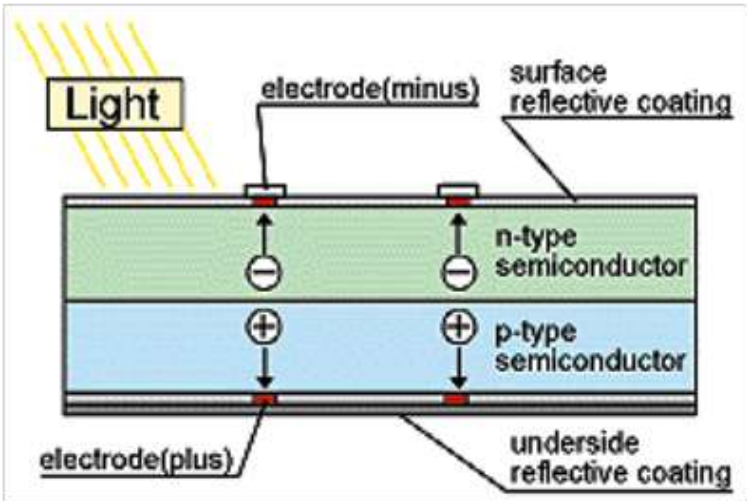

Figure (2-4) Photovoltaic energy

(2.4) Photovoltaic cell

A device that produces an electric reaction to light, producing electricity . PV cells do not use the sun's heat to produce electricity. They produce electricity directly when sunlight interacts with semiconductor materials in the PV cells.

(2.5) Photovoltaic characteristics

Voltage and Current outputs of the PV modules are affected by temperature and irradiance [4].Power electronics components of a photovoltaic system, such as grid-direct inverters have maximum and minimum voltage inputs. During rating of power electronics equipment, these variations should be taken into account especially for the MPPT range of inverters.

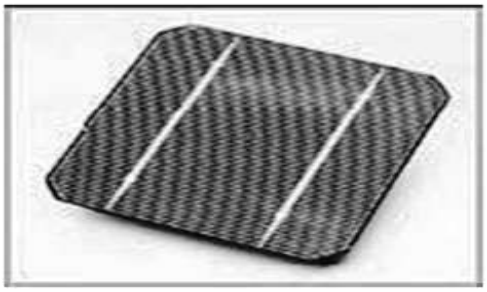

Figure (2-5) PV cell

(2.6) Principle of Operation of PV cell

Solar cell is a device which converts photons in Solar rays to direct-current (DC) and voltage. The associated technology is called Solar Photovoltaic (SPV). A typical silicon PV cell is a thin wafer consisting of a very thin layer of phosphorous-doped (N-type) silicon on top of a thicker layer of boron-doped (P-type) silicon. An electrical field is created near the top surface of the cell where these two materials are in contact (the P-N junction).

When the sunlight hits the semiconductor surface, an electron springs up and is attracted towards the N-type semiconductor material. This will cause more negatives in the n-type and more positives in the P-type semiconductors, generating a higher flow of electricity. This is known as Photovoltaic effect.

A PV array is made up of a number of solar modules connected together. A solar module is made up of a number of solar cells. Solar cells are composed of silicon (Si). Silicon is a semi-conductor with only four electrons in its outer shell. When a photon of solar radiation from the sun strikes an outer shell electron, a transfer of energy takes place. The incoming photon losses

the amount of energy required to eject an electron from its shell and therefore a free electron is produced. This phenomenon is known as the photoelectric effect. [28]The performance of a solar cell is dependent on its output voltage and current and how they vary with each other. The typical I-V curve for a solar cell is not a straight line as expected by it is as shown in the figure below, A PV module's voltage output is actually a variable value that is primarily affected by temperature. The relationship between module voltage and temperature is actually an inverse one. As PV module manufacturers will report the amount of change their modules experience in the form of temperature coefficients, most often in terms of a percentage per degree Celsius. For example for BP solar modules at NTNU, the open circuited voltage temperature coefficient is − 0.086/oC. This means that for every degree change in temperature, the module's open circuited voltage, Voc will change in the opposite direction by 8.6%. For example, if the PV module got colder by 1°C, the PV voltage would increase by 8.6%.To illustrate this phenomenon, let's consider the worst case of temperatures recorded in it shows for the data recorded the average maximum temperature was 14.4°C with irradiance of 123W/m2 h in the month of August. On the other hand the minimum average temperature was obtained in January and the data recorded was -3.4°C with irradiance of 18W/m2 h. The formula in can be used to determine the averaged maximum and minimum voltages of the modules at these temperatures.Since the stringvoltage in this design will have a voltage,Voc is obtained to be300 V.

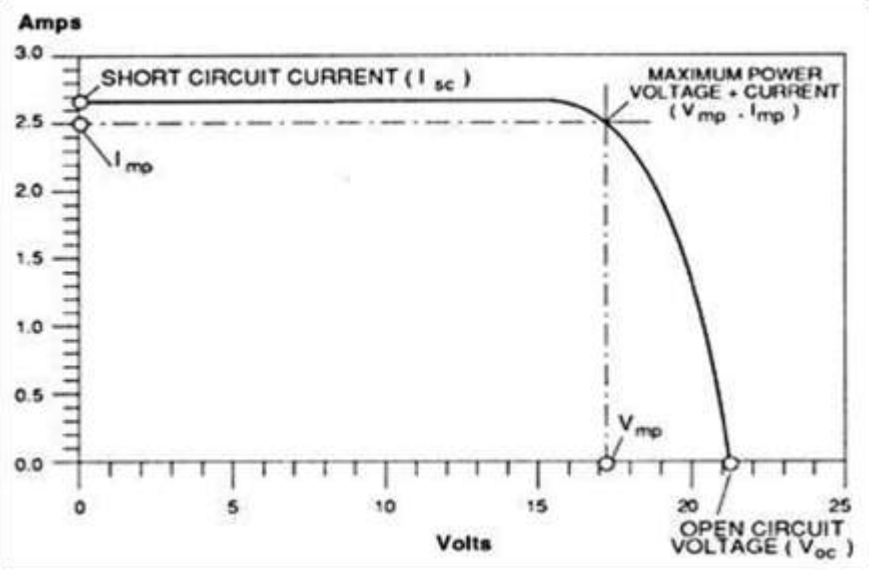

Figure (2-6) Current and Voltage characteristics of a PV module with temperature variation

(2.7) Solar Cell Efficiency

There are three variables use to study the efficiency solar cell from p-n junction it conceder the basic output of the solar cell

(2.7.1) Short Circuit Current (Isc)

The cells are characterized by many parameters, one of these parameter, is the short-current it is defined as the current that flows when the cells terminals are connected with resistant less wire. The short circuit current (Isc) that passes through the junction under elimination when the voltage is equal to zero and the maximum short circuit current that generate from the material of solar cell that join by the flux of incident photon that possess the maximum energy from energy band gap of the metal that can enable to generate the ion pairs (electron-hole) we can calculate solar cell by the silicon energy gap that equal 1.24volts as the equation

$$E_{gap} = \frac{1.24}{\lambda} \qquad (2.1)$$

To find whenever the energy gap is very narrow the short current density is large because the incident photon possess enough energy to create ion pairs (electron-hole) when the energy band gap is less than its energy.

Once the light is incident to the junction of solar cell the current is from the equation

$$I = I_0\left(e^{\beta V} - 1\right) - I_P \qquad (2.2)$$

Where $I_0$the saturation current, V is the voltage and I_P is the photon current

In this case V=0 and $I = I_{sc}$ and equation (2.2) gives:

$$I_{sc} = I_o(e^0 - 1) - I_P = -I_P \qquad (2.3)$$

$$I_{sc} = -I_P \qquad (2.4)$$

(2.7.2) Open –Circuit Voltage (V_{oc})

The other parameter is the so called open circuit voltage V_{oc} it is defined as the volt, when no current flows. It can calculate the open voltage circuit (V_{oc}) of solar cell from ideal p-n junction from the equations:

$$\text{At} \quad I = 0\,, \; V = V_{oc} \qquad (2.5)$$

$$I = I_0\left(e^{\beta V} - 1\right) - I_P$$

$$0 = I_0\left(e^{\beta V_{oc}} - 1\right) - I_P$$

$$e^{\beta V_{oc}} = \frac{I_o + I_P}{I_0} = 1 + \frac{I_P}{I_0}$$

$$V_{oc} = \frac{1}{\beta}\ln(1 + \frac{I_P}{I_0}) \qquad (2.6)$$

To determinate the maximum voltage (V_{oc}) it must being I_P is very small and the acceptability estimations to minimum saturated current I_P as a function of energy gap is

$$I_P = 1.5 \times 10^5 \exp\left(\frac{-E_g}{KT}\right) A/cm \qquad (2.7)$$

This relation determine the maximum value of voltage V_{oc} it decreases with decreases of energy gap this direction is the opposite case of the open circuit current Isc and from shows there is ideal energy gap to find the maximum efficiency.

(2.7.3) Fill-Factor (FF)

The short circuit current and the open circuit voltage are the maximum current and voltage respectively from a solar cell. However, at both of these operating points, the power from the solar cell is zero. The fill factor, more commonly known by its abbreviation "FF", is a parameter which, in conjunction with V_{oc} and Isc determines the maximum power from a solar cell. The FF is defined as the ratio of the maximum power from the solar cell to the product of V_{oc} and Isc graphically:

$$FF = \frac{V_m I_m}{V_{oc} I_{sc}} \qquad \frac{Pmax}{V_{oc} I_{sc}} \qquad (2.8)$$

Where FF is the fill factor.

The fill factor considers to a stander tidal referential of output characterization and its value for solar cell of the acceptable efficiency by the range between 0.7-0.85.

(2.7.4) Calculation of I_{max} and V_{max}

To calculate the voltage at the maximum power $V_{max}$and the current at the maximum power I_{max}it can be started from equations of power:

$$P = IV = VI_0\left(e^{\beta V} - 1\right) - VI_P \qquad (2.9)$$

And by knowing the three parameters we can calculate the solar cells efficiency [26]

$$\eta = \frac{V_m I_m}{P_{in}} = \frac{V_{oc} I_{sc}}{P_{in}}$$

(2.8) Optical Properties

Optical property of a material is defined as its interaction with electromagnetic radiation in the visible. Optical properties of materials are essential for optical science research and industrial

applications. The interaction of light with matter is different at different wavelengths and the techniques to measure the optical properties differ based on the spectral region of interest.

The optical properties exhibited by nanomaterials are quite different from their bulk counterpart. The reason behind this change in property is mainly due to the effect of the surface. In addition to, the increased energy level spacing is also an important criterion for this changing behavior, which effect by doping and interaction with the surrounding environment or other nanostructures.[27, 28]

(2.8. 1) Optical Processes of Light

When radiation interacts with matter, a number of processes can occur; including reflection, scattering, absorbance, Fluorescence, and photochemical reaction (absorbance and bond breaking).

The crystals are composed of charged particles: bound and conduction electrons, ionic cores, impurities, etc. These particles move differently with oscillating electric fields, giving rise to polarization effects. At visible and infrared light frequencies, the only contribution to polarization comes from the displacement of the electron cloud, which produces an induced dipole moment. According to that the charged particles obey on the equations of motion, and they give rise to fields in accordance with Maxwell's theory of electrodynamics. The interaction of the electromagnetic radiation with these crystals is treated, by applying the boundary conditions to the solutions of the Maxwell equations at the boundary between the different media. Two quantity used to describe electromagnetic fieldare electric field (E) and magnetic field (H).

Maxwell equations: [29]

$$\mathrm{H} - \frac{1}{\mathrm{C}}\frac{\partial \mathrm{D}}{\partial \mathrm{t}} = \frac{4\pi}{\mathrm{C}}\mathrm{J}$$

$$\nabla \times \mathrm{E} + \frac{1}{\mathrm{C}}\frac{\partial \mathrm{B}}{\partial \mathrm{t}} = 0$$

$$\nabla \cdot \mathrm{E} = 0$$

$$\nabla \cdot \mathrm{B} = 0 \qquad (2.16)$$

(2.8. 2) Reflection of Light

When light passes from one transparent medium to another having a different index of refraction, some of it is reflected off a surface (such as a mirror), since the angle of incidence on a reflecting basic surface is equal to the angle of reflection (reflectionlaw).

(2.8. 3) Refraction of Light

When light is incident at interface, the geometrical plane that separates one optical medium from anther, it will be partly reflected and partly transmitted and refracted into second medium. The bending waves of light at interface between two optical mediums called refraction.

(2.8 4) Transmission of Light

The transition of light that intensity of light transmitted out of the substance. The quantity related with transmission of light is transmittance which means quantity of light that is passes through sample. Transmittance is determined by the relationship between amount of light that is transmitted and original of light this expressed in following formula:

$$T = \frac{I}{I_0} \qquad (2.17)$$

(2.8. 5) Absorption of Light

Absorption is light which absorbed by sample. The quantity related with absorption of light is absorbance which means amount of light absorbed by sample.

Absorbance is determine by the relationship between amount of light that original of light is and transmitted light this expressed in following formula [30, 31,32]

$$A = \frac{I_0}{I} \qquad (2.18)$$

Beer – Lambert law is discussed relationship between the amount of light transmitted and the thickness of the sample. It was stated that, the absorbance of a solution is directly proportional to the thickness and the concentration of the sample, as follows:

$$A = \alpha ct \qquad (2.19)$$

Where: A is absorbance.

C is concentration.

t is path length (thickness).

αis absorbance coefficient or molar absorptivity (Lmol-1 cm1)

In spectrophotometry the absorbance and transmittance are often related together. The ray of light with intensity (I0) comes into material, the material will absorb part of the light (Ia) and the other remaining light will transmit (It). That expresses as follows:

$$I = I_a + I_t \qquad (2.20)$$

When using percentage transmittance values, it is easy to relate and to understand the numbers. For example, 50% transmittance means that half of the light is transmitted and half is absorbed,

while 75% transmittance means that three quarters of the light is transmitted and one quarter absorbed. Completely transparent substance will have It=I0 and its Transmittance is will be 100% and its absorbance is zero. Similarly a substance which no allow radiation of particular wavelength to pass through it will It=0 and corresponding to zero percent transmittance and its absorbance is 100%. Thus the relationship between absorbance (α) and Transmittance (T) can be expressed by the following : [33, 34]

$$A = \frac{1}{T} = \frac{I_0}{I} \qquad (2.21)$$

Absorbance (A), then, is defined as the logarithm (base 10) of the reciprocal of the transmittance.

$A = -\log_{10} T$

$$A = -\log_{10} \qquad (2.22)$$

The Beer – Lambert law in exponential formula can be written as following:

From (2.19) and (2.22)

$$A = -\log_{10}\left(\frac{I}{I_0}\right) = \alpha ct$$

For concertation one mole, c=1.

$$A = \log_{10}\left(\frac{I}{I_0}\right) = -\alpha t \qquad (2.23)$$

Light loses intensity in absorbed material according Beers law given as following:

By take the exponential for equation (2.23)

$$\frac{I}{I_0} = e^{-\alpha t}$$

This equation may be rewrite as,

$$I = I_0 e^{-\alpha t} \qquad (2.24)$$

Where α is absorbance coefficient.

ttis thickness of matter.

I0, I, are intensity of absorption and transition light.

The absorption coefficient □ can be related to the band gap. Tauc derived an expression that gives the relation between absorption coefficient α and the incident photon energyhυ. According the fallowing relation:

$$\alpha h\upsilon \propto \Delta E^n \qquad (2.25)$$

Absorption operation depend on energy of photon hυ and energy gap Eg. If energy of photon hυ equal to energy gap Eg, photon will absorbed to generate pairs of electron –hole. If energy of photon hυ less than energy gap Eg, photon will not absorbed. If energy of photon hυ greater than energy gap Eg, electron will exiting from valance band to conductor band since the difference in energy $h\upsilon - Eg$ will released in heat form [35, 36,37]

$$\Delta E = h\upsilon - E_g \qquad (2.26)$$

From (2.25) and (2.26)

$$\alpha h\upsilon = c\left(h\upsilon - E_g\right)^n \qquad (2.27)$$

Where hυ is the photon energy.

Eg is the optical band gap (the threshold for photons to be absorbed).

c is a proportionality constant depend on sort of matter.

n is the index indicating the type of transition.

(2.9) The Optical Constants

Optical constants any several quantities characteristic of the optical behavior of substance as refractive index, absorption coefficient, dielectric constant, extinction coefficient and optical conductivity, which are response coefficients of matter to an incident electromagnetic wave of circular frequency ω. The optical constant will vary for different wave lengths, so it can be used to predict the material's response to each wave length [38].

(2.10) The Absorption Coefficient (α)

The absorption coefficient (α) measures the intensity loss of the electromagnetic radiation, as it passes through substance [39, 40].

The absorption coefficient can be obtained by taken the logarithm for equation (2.14)

$$\log_{10}\frac{I}{I_0} = -\alpha t \log_{10} e$$

By substitute equation (2.22)

$$A = \alpha t \log_{10} e$$

$$\alpha = \frac{A}{t\log_{10} e} = \frac{2.303A}{t}$$

$$\alpha = \frac{2.303A}{t} \qquad (2.28)$$

(2.11) Extinction Coefficient

Extinction coefficient is measure of light lost due to scattering and absorption per unit distance of the penetration medium. It can be obtained from the following equations [41]

Starting with electric field formula;

$$E(z,t) = E_0 e^{i(Kz-\omega t)} \qquad (2.29)$$

The value of wave number given by:

$$k = \frac{2\pi}{\lambda/_n} = \frac{n\omega}{c} \Rightarrow k = n\frac{\omega}{c}$$

$$\text{And } \frac{2\pi}{\lambda/_n} = \frac{n\omega}{c} \Rightarrow \omega = \frac{2\pi c}{\lambda} \qquad (2.30)$$

n is complex index, which include two important optical properties index, n0 is the real part; related to the refraction, and k0 is the imaginary part; related to the attenuation of incident light (extinction coefficient).

So complex index of refraction of the medium n is defined as:

$$n = n_0 + ik_0 \qquad (2.31)$$

$n_0$is real index refraction.

$k_0$is extinction coefficient.

Then k from equation (2.31), became:

$$k = (n_0 + ik_0)\frac{\omega}{c} \qquad (2.32)$$

Substitute equation (2.32) in equation (2.29)

$$E(z,t) = E_0 e^{i\left(\frac{(n_0+ik_0)\omega z}{c}-\omega t\right)}$$

$$= E_0 e^{\frac{-k_0\omega z}{c}} e^{i\left(\frac{\omega n_0 z}{c}-\omega t\right)}$$

$$= E_0 e^{\left(\frac{-k_0\omega z}{c} + i\left(\frac{\omega n_0 z}{c}-\omega t\right)\right)} \qquad (2.33)$$

The complex conjugate of electric field given by:

$$E^* = E_0 e^{\left(\frac{-k_0\omega z}{c} - i\left(\frac{\omega n_0 z}{c}-\omega t\right)\right)} \qquad (2.34)$$

$$\because I \propto EE^*$$

From equation (2.33) and (2.34)

$$I \propto E_0 e^{\left(\frac{-k_0\omega z}{c} + i\left(\frac{\omega n_0 z}{c}-\omega t\right)\right)} \cdot e^{\left(\frac{-k_0\omega z}{c} - i\left(\frac{\omega n_0 z}{c}-\omega t\right)\right)}$$

$$I \propto E_0 e^{\left(\frac{-2k_0\omega z}{c}\right)} \qquad (2.35)$$

By comparative equation (2.35) with equation (2.24), here z is acts the thickness t, the absorption coefficient(α) equals:

$$\alpha = \frac{2k_0\omega}{c}$$

Then substitute the value of ω from equations (2.30),

$$\alpha = \frac{2k_0\omega}{c} = \frac{4\pi k_0}{\lambda} \qquad (2.36)$$

So the extinction coefficient (k_0) equals:

$$k_0 = \frac{\lambda\alpha}{4\pi} \qquad (2.37)$$

(2.12) Refraction Index

The refractive index (n) is the relative between speeds of light in vacuum to its speed in material which does not absorb this light. The value of n can be calculated from the equation [42, 43].

$$n = \left[\left(\frac{(1+R)}{(1-R)}\right)^2 - (1 + k_0^2)\right]^{\frac{1}{2}} + \frac{(1+R)}{(1-R)}\Bigg] \qquad (2.38)$$

Where (R) is the reflectivity. k0 is extinction coefficient

(2.13) Dielectric Constant

As electromagnetic wave interact with dielectric medium, polarization of the medium occurs and this is dependent on the permittivity of the medium. To find out what kind of electromagnetic waves exist inside the dielectric medium, use Maxwell equations obtains the well-known formula for refractive index under assumptions that there are no free charge $\nabla \cdot E = 0$, no currents $\nabla \cdot B = 0$ and all materials are non-magnetic $\mu = 0$ incase Maxwell equations reduce to wave vector equations the solution will be propagating wave . [44, 45].

$$\nabla^2 E - \frac{\varepsilon}{c^2}\frac{\partial^2 E}{\partial t^2} = 0$$

$$\nabla^2 B - \frac{\varepsilon}{c^2}\frac{\partial B}{\partial t} = 0 \qquad (2.39)$$

The solutions to these equations, we assume that electric field have the form of harmonic plane waves with the wave vector k,

$$E = E_0 \exp i(\omega t - kz) \qquad (2.40)$$

εis relative permittivity, c is the velocity of light.

Where E0 is amplitude, wave velocity.

Substitute equation (2.39) in equation (2.40) and diffraction in z direction $\left(-ik\right)^2 e^{i(\omega t-kz)} - \frac{\varepsilon}{c^2}(i\omega)^2 e^{i(\omega t-kz)} = 0$

$$-k^2 + \frac{\varepsilon}{c^2}\omega^2 = 0 \implies \omega = ck\varepsilon^{-\frac{1}{2}} \quad (2.41)$$

The phase velocity of the wave

$$v = \frac{\omega}{k} \quad (2.42)$$

From (2.41) and (2.42)

$$v = \frac{\omega}{k} = c\varepsilon^{\frac{-1}{2}} = \frac{c}{n} \quad (3.43)$$

The equation (2.33) can be written as fallows, properties.

$$\varepsilon = n^2 \quad (2.44)$$

This indicate the dielectric constant is directly related to the optical properties.

In general, the dielectric constant ε are complex quantities, that is,

$$\varepsilon = \varepsilon_1 - i\varepsilon_2 \quad (2.45)$$

$\varepsilon_1$is real dielectric Constant.

$\varepsilon_2$is imagery dielectric Constant.

It is useful to define a complex index of refraction from

From equation (2.31), equation (2.44) and equation (2.45),

$$\varepsilon_1 - i\varepsilon_2 = (n_0 - ik_0)^2 = n_0^2 - 2nki - k_0^2$$

$$\varepsilon_1 - i\varepsilon_2 = n_0^2 - 2n_0 k_0 i - k_0^2 \quad (2.46)$$

Thus from equation (2.46)

The real Dielectric Constant (ε1)

$$\varepsilon_1 = n_0^2 - k_0^2 \quad (2.47)$$

The imaginary dielectric constant (ε2)

$$\varepsilon_2 = 2n_0 k_0 \quad (2.48)$$

(2. 14) Optical Conductivity

The optical conductivity is a measure of frequency response of material when irradiated with light.

The dielectric constant is related to the optical conductivity. In order to derive the relation between the dielectric constant and the optical conductivity. We assume that electric field is oscillating with angular frequency ω.

$$E(z,t) = E_0 e^{i(Kz-\omega t)} \qquad (2.49)$$

This wave propagates through the medium with conductivity σ (ω) and the dielectric constant ε (ω), both being the function of ω. This implies the polarization of the medium occurs only due to the bound charges (polarization due to ions). The electric current and the electrical displacement are related to the electric field by the fallows relations [46, 47].

$$J = \sigma E$$

$$D = \varepsilon E \qquad (2.50)$$

We could start with the equation of motion for electrons:

$$\nabla^2 E = \frac{\varepsilon\mu}{C^2}\frac{\partial^2 E}{\partial t^2} + \frac{4\pi\sigma\mu}{C^2}\frac{\partial E}{\partial t} \qquad (2.51)$$

$$\nabla^2 H = \frac{\varepsilon\mu}{C^2}\frac{\partial^2 H}{\partial t^2} + \frac{4\pi\sigma\mu}{C^2}\frac{\partial H}{\partial t} \qquad (2.52)$$

Substitute equations (2.49) and (2.40) in equation (2.51) and take the diffraction in z – direction.

$$-k^2 = -\frac{\varepsilon\mu\omega^2}{C^2} - \frac{4\pi i\sigma\mu\omega}{C^2} \qquad (2.53)$$

We may rewrite equation (2.53) in the form

$$k^2 = \frac{\omega^2}{C^2}\mu\left(\varepsilon + \frac{4\pi i\sigma}{\omega}\right) \qquad (2.54)$$

If there were no losses (or no attenuation), k would be equal to

$$k_0 = \frac{\omega}{c}\sqrt{\varepsilon\mu} \qquad (2.55)$$

And would be real, but since there are losses we write

$$k = \frac{\omega}{c}\sqrt{\varepsilon_{complex}\mu} \qquad (2.56)$$

Where we have defined the complex dielectric function as

$$\varepsilon_{complex} = \varepsilon_1 + i\varepsilon_2 = \varepsilon + \frac{4\pi i\sigma_{opt}}{\omega} \qquad (2,57)$$

So the imaginary dielectric part

$$\varepsilon_2 = \frac{4\pi\sigma_{opt}}{\omega}$$

Then optical conductivity from equation(2.57)

$$\sigma_{opt} = \frac{\varepsilon_2\omega}{4\pi} \qquad (2.58)$$

By substitute ε_2 from equation (2.48)

$$\sigma_{opt} = \frac{2n_0 k_0 \omega}{4\pi}$$

$$\sigma_{opt} = \frac{2k_0 \omega n_0}{4\pi} \quad (2.59)$$

The absorption coefficient from equation (2.36) equals,

$$\alpha = \frac{2k_0 \omega}{c}$$

$$\alpha c = 2k_0 \omega \quad (2.60)$$

Then optical conductivity can be obtained by:

$$\sigma_{opt} = \frac{\alpha c n_0}{4\pi} \quad (2.61)$$

(2 15) Electrical Properties

Electrical properties of materials are their ability to conduct electrical current. Various electrical properties such are resistivity, electrical conductivity and dielectric sterngth.

Reduction in material's dimensions would have effects on electrical properties. In bulk materials, conduction of electrons is delocalized, that is, electrons can move freely in all directions. When the scale is reduced to nanoscale, the quantum effect dominates. For zero dimensional nanomaterials, all the dimensions are at the nanoscale and hence the electrons are confined in three dimensional space. Therefore no electron delocalization (freedom to move) occurs. For one dimensional nanomaterials, electrons confinement occurs in two dimensional space and hence electron delocalization takes place along the axis of nanotubes, Nano rods, or nanowires. In the case of two dimensional nanomaterials, the conduction electrons will be confined across the thickness but delocalized in the plane of the sheet. Due to electron confinement, the energy bands are replaced by discrete energy states which make the conducting materials to behave like either semiconductors or insulators [48]. Here we shall discuss two important electrical properties related to spectroscopy studies;

(2.15. 1) Electric Conductivity

The electrical conductivity is measure of materials ability to allow the transport of an electric charge. It can be estimated using the following relation [49].

$$\sigma_{ele} = \frac{2\lambda\sigma_{opt}}{\alpha} \quad (2.62)$$

(2.15. 2) Permittivity

Permittivity is measure of well the molecules of substance align polarize under electric field. This value calculated from the relation:

$$\varepsilon_r = \frac{8.85x10^{-12}}{\sqrt{n}} \qquad (2.63)$$

where n is refractive index.

(2.15. 3) Magnetic Properties

Magnetic property refers response of material to an applied magnetic field. The magnetic properties of solid known as magnetism arises from dipole moment in solids. This dipole moment appears from the spinning of electrons in its axis and orbital motion around the nucleus of atom. The magnetic properties of solid are observed due to the magnetic field created by electrons, magnetic moment and electric current.

(2.15. 4) Permeability

Magnetic permeability is property exhibit by the material where the material allows of magnetic lines of force to pass through it. It can be calculated from the relation [50].

(2.16) Nano materials

Nanomaterials are materials which are characterised by an ultra-fine grain size (< 50 nm) or by a dimensionality limited to 50 nm.

Nanomaterials and Nanotechnologies attract tremendous attention in recent researches. New physical properties and new technologies both in sample preparation and device fabrication evoke on account of the development of nanoscience. Various research fields including physics, chemists, material scientists, and engineers of mechanical and electrical are involved in this research. In this review various methods of preparing nanomaterials including insulators, semiconductors, and metals are discussed. We express the exotic physical properties concerning the linear and nonlinear optical spectra, temperature dependence of resistivities, spin resonance spectra, and magnetic susceptibility measurements**.**[51]Anumber of fascinating and provocative results have been developed that lead our perspective understanding of quantum tunneling, quantum phase transition, surface effect, quantum size-effect confinement and nonlinear susceptibility enhancements. Nanomaterials are cornerstones of nanoscience and nanotechnology. Nanostructure science and technology is a broad and interdisciplinary area of research and development activity that has been growing explosively worldwide in the past few years. It has the potential

for revolutionizing the ways in which materials and products are created and the range and nature of functionalities that can be accessed. It is already having a significant commercial impact, which will assuredly increase in the future.

Nanoscale materials are defined as a set of substances where at least one dimension is less than approximately 100 nanometers. A nanometer is one millionth of a millimeter - approximately 100,000 times smaller than the diameter of a human hair. Nanomaterials are of interest because at this scale unique optical, magnetic, electrical,

and other properties emerge. These emergent properties have the potential for great impacts in electronics, medicine, and other fields.

Figure (.2- 7) Nanomaterial (For example: Carbon nanotube)

Some nanomaterials occur naturally, but of particular interest are engineered nanomaterials (EN), which are designed for, and already being used in many commercial products and processes. They can be found in such things as sunscreens, cosmetics, sporting goods, stain-resistant clothing, tires, electronics, as well as many other everyday items, and are used in medicine for purposes of diagnosis, imaging and drug delivery. Engineered nanomaterials are resources designed at the molecular (nanometre) level to take advantage of their small size and novel properties which are generally not seen in their conventional, bulk counterparts. The two main reasons why materials at the nano scale can have different properties are increased relative surface area and new quantum effects. Nanomaterials have a much greater surface area to volume ratio than their conventional forms, which can lead to greater chemical reactivity and affect their strength. Also at the nano scale, quantum effects can become much more important in determining the materials properties and characteristics, leading to novel optical, electrical and

magnetic behaviours. Nanomaterials are already in commercial use, with some having been available for several years or decades. The range of commercial products available today is very broad, including stain-resistant and wrinkle-free textiles, cosmetics, sunscreens, electronics, paints and varnishes. Nanocoatings and nanocomposites are finding uses in diverse consumer products, such as windows, sports equipment, bicycles and

automobiles. There are novel UV-blocking coatings on glass bottles which protect beverages from damage by sunlight, and longer-lasting tennis balls using butylrubber/ nano-clay composites. Nanoscale titanium dioxide, for instance, is finding applications in cosmetics, sun-block creams and self-cleaning windows, and nanoscale silica is being used as filler in a range of products, including cosmetics and dental fillings.

(2.16. 1) Advances in Nanomaterials

The history of nanomaterials began immediately after the big bang when Nanostructures were formed in the early meteorites. Nature later evolved many other Nanostructures like seashells, skeletons etc. Nanoscaled smoke particles were formed during the use of fire by early humans. The scientific story of nanomaterials however began much later. One of the first scientific report is the colloidal gold particles synthesised by Michael Faraday as early as 1857. Nanostructured catalysts have also been investigated for over 70 years. By the early 1940's, precipitated and fumed silica nanoparticles were bein manufactured and sold in USA and Germany as substitutes for ultrafine carbon black for rubber reinforcements. Nanosized amorphous silica particles have found large-scale applications in many every-day consumer products, ranging from non-diary coffee creamer to automobile tires, optical fibers and catalyst supports. In the 1960s and 1970's metallic nanopowders for magnetic recording tapes were developed. In 1976, for the first time, nanocrystals

produced by the now popular inert- gas evaporation technique was published by Granqvist and Buhrman. Recently it has been found that the Maya blue paint is ananostructured hybrid material. The origin of its color and its resistance to acids and biocorrosion are still not understood but studies of authentic samples from Jaina Island show that the material is made of needle-shaped palygorskite (clay) crystals that form a superlattice with a period of 1.4 nm, with intercalates of amorphous silicate substrate containing inclusions of metal (Mg) nanoparticles. The beautiful tone of the blue color is obtained only when both these nanoparticles and the superlattice are present, as has been shown by the fabrication of synthetic samples.

Today nanophase engineering expands in a rapidly growing number of structural and functional materials, both inorganic and organic, allowing to manipulate mechanical, catalytic, electric, magnetic, optical and electronic functions.The production of

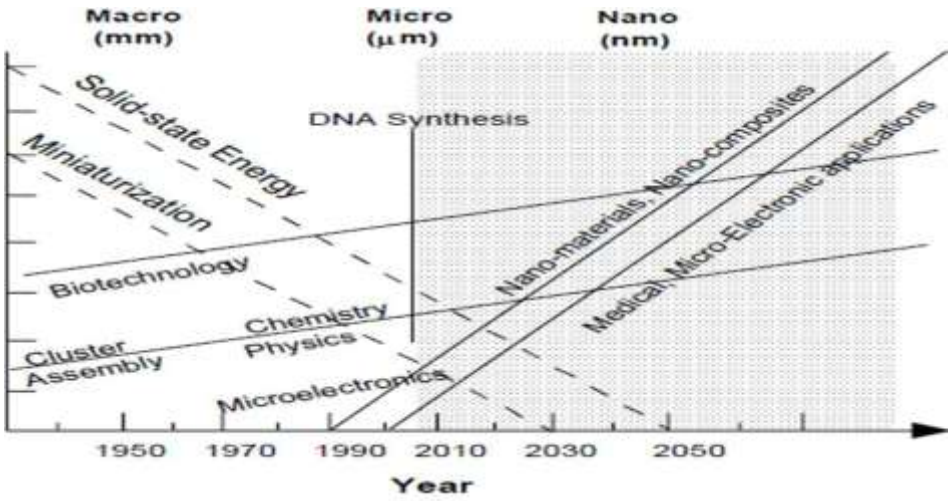

Figure (2.8)

nanophase or cluster-assembled materials is usually based upon the creation of separated small clusters which then are fused into a bulk-like material or on their embedding into compact liquid or solid matrix materials. e.g. nanophase silicon, which differs from normal silicon in physical and electronic properties, could be applied to macroscopic semiconductor processes to create new devices. For instance, when ordinary glass is doped with quantized semiconductor "colloids," it becomes a high performance optical medium with potential applications in optical computing.

(2.16.2) Properties of Nanomaterials

Nanomaterials have the structural features in between of those of atoms and the bulk materials. While most microstructured materials have similar properties to the corresponding bulk materials, the properties of materials with nanometer dimensions are significantly different from those of atoms and bulks materials. This is mainly due to the nanometer size of the materials which render them: (i) large fraction of surface atoms; (ii) high surface energy; (iii) spatial confinement; (iv) reduced imperfections, which do not exist in the corresponding bulk materials. Due to their small dimensions, nanomaterials have extremely large surface area to volume ratio, which makes a large to be the surface or interfacial atoms, resulting in more “surface” dependent

material properties. Especially when the sizes of nanomaterials are comparable to length, the entire material will be affected by the surface properties of nanomaterials. This in turn may enhance or modify the properties of the bulk materials. For example, metallic nanoparticles can be used as very active catalysts. Chemical

sensors from nanoparticles and nanowires enhanced the sensitivity and sensor selectivity. The nanometer feature sizes of nanomaterials also have spatial confinement effect on the materials, which bring the quantum effects. The energy band structure and charge carrier density in the materials can be modified quite differently from their bulk and in turn will modify the electronic and optical properties of the materials. For example, lasers and light emitting diodes (LED) from both of the quantum dots and quantum wires are very promising in the future optoelections. High density information storage using quantum dot devices is also a fast developing area. Reduced imperfections are also an important factor in determination of the properties of the nanomaterials. Nanosturctures and Nanomaterials favors of a selfpurification process in that the impurities and intrinsic material defects will move to near the surface upon thermal annealing. This increased materials perfection affects the properties of nanomaterials. For example, the chemical stability for certain nanomaterials may be enhanced, the mechanical properties of nanomaterials will be better than the bulk materials. The superior mechanical properties of carbon nanotubes are well known. Due to their nanometer size, nanomaterials are already known to have many novel properties. Many novel applications of the nanomaterials rose from these novel properties have also been proposed.

(2.16.3) Optical properties of Nanomaterials

One of the most fascinating and useful aspects of nanomaterials is their optical properties. Applications based on optical properties of nanomaterials include optical detector, laser, sensor, imaging, phosphor, display, solar cell, photocatalysis, photo electrochemistry and biomedicine. The optical properties of nanomaterials depend on parameters such as feature size, shape, surface characteristics, and other variables including doping and interaction with the surrounding environment or other nanostructures. Likewise, shape can have dramatic influence on optical properties of metal nanostructures. exemplifies the difference in the optical properties of metal and semiconductor nanoparticles. With the CdSe semiconductor nanoparticles, a simple change in size alters the optical properties of the nanoparticles. When metal nanoparticles are enlarged, their optical properties change only slightly as observed for the different samples of gold

nanospheres , when an anisotropy is added to the nanoparticle, such as growth of nanorods, the optical properties of the nanoparticles change dramatically.

(2.16. 4) Electrical properties of Nanomaterials

Electrical Properties of Nanoparticles" discuss about fundamentals of electrical conductivity in nanotubes and nanorods, carbon nanotubes, photoconductivity of nanorods, electrical conductivity of nanocomposites. One interesting method which can be used to demonstrate the steps in conductance is the mechanical thinning of a nanowire and measurement of the electrical current at a constant applied voltage. The important point here is that, with decreasing diameter of the wire, the number of electron wave modes contributing to the electrical conductivity is becoming increasingly smaller by well-defined quantized steps. In electrically conducting carbon nanotubes, only one electron wave mode is observed which transport the electrical current. As the lengths and orientations of the carbon nanotubes are different, they touch the surface of the mercury at different times, which provides two sets of information: (i) the influence of carbon nanotube length on the resistance; and (ii) the resistances of the different nanotubes. As the nanotubes have different lengths, then with increasing protrusion of the fiber bundle an increasing number of carbon nanotubes will touch the surface of the mercury droplet and contribute to the electrical current transport.

(2.16. 5) Mechanical properties of Nanomaterials

"Mechanical Properties of Nanoparticles" deals with bulk metallic and ceramic materials, influence of porosity, influence of grain size, superplasticity, filled polymer composites, particle-filled polymers, polymer-based nanocomposites filled with platelets, carbon nanotube-based composites. The discussion of mechanical properties of nanomaterials is, in to some extent, only of quite basic interest, the reason being that it is problematic to produce macroscopic bodies with a high density and a grain size in the range of less than 100 nm. However, two materials, neither of which is produced by pressing and sintering, have attracted much greater interest as they will undoubtedly achieve industrial importance. These materials are polymers which contain nanoparticles or nanotubes to improve their mechanical behaviors, and severely plastic-deformed metals, which exhibit astonishing properties. However, because of their larger grain size, the latter are generally not accepted as nanomaterials. Experimental studies on the mechanical properties of bulk nanomaterials are generally impaired by major experimental problems in producing specimens with exactly defined grain sizes and porosities. Therefore, model

calculations and molecular dynamic studies are of major importance for an understanding of the mechanical properties of these materials. Filling polymers with nanoparticles or nanorods and nanotubes, respectively, leads to significant improvements in their mechanical properties. Such improvements depend heavily on the type of the filler and the way in which the filling is conducted. The latter point is of special importance, as any specific advantages of a Nano particulate filler may be lost if the filler forms aggregates, thereby mimicking the large particles. Particulatefilled polymer-based Nano composites exhibit a broad range of failure strengths and strains. This depends on the shape of the filler, particles or platelets, and on the degree of agglomeration. In this class of material, polymers filled with silicate platelets exhibit the best mechanical properties and are of the greatest economic relevance. The larger the particles of the filler or agglomerates, the poorer are the properties obtained. Although, potentially, the best composites are those filled with nanofibers or nanotubes, experience teaches that sometimes such composites have the least ductility. On the other hand, by using carbon nanotubes it is possible to produce composite fibers with extremely high strength and strain at rupture. Among the most exciting nanocomposites are the polymerceramic nanocomposites, where the ceramic phase is platelet-shaped. This type of composite is preferred in nature, and is found in the structure of bones, where it consists of crystallized mineral platelets of a few nanometers thickness that are bound together with collagen as the matrix. Composites consisting of a polymer matrix and defoliated phyllosilicates exhibit excellent mechanical and thermal properties.

(2.16.6) Magnetic properties of Nanomaterials

Bulk gold and Pt are non-magnetic, but at the nano size they are magnetic. Surface atoms are not only different to bulk atoms, but they can also be modified by interaction with other chemical species, that is, by capping the nanoparticles. This phenomenon opens the possibility to modify the physical properties of the nanoparticles by capping them with appropriate molecules. Actually, it should be possible that non-ferromagnetic bulk materials exhibit ferromagnetic-like behavior when prepared in nano range. One can obtain magnetic nanoparticles of Pd, Pt and the surprising case of Au (that is diamagnetic in bulk) from non-magnetic bulk materials. In the case of Pt and Pd, the ferromagnetism arises from the structural changes associated with size effects.

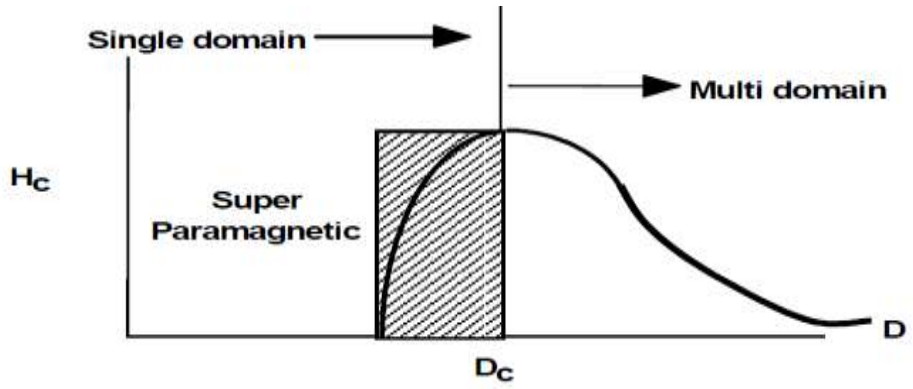

Figure (.2. 9) Magnetic properties of nanostrucutred materials

However, gold nanoparticles become ferromagnetic when they are capped with appropriate molecules: the charge localized at the particle surface gives rise to ferromagnetic-like behavior. Surface and the core of Au nanoparticles with 2 nm in diameter show ferromagnetic and paramagnetic character, respectively. The large spin-orbit coupling of these noble metals can yield to a large anisotropy and therefore exhibit high ordering temperatures. More surprisingly, permanent magnetism was observed up to room temperature for thiol-capped Au nanoparticles. For nanoparticles with sizes below 2 nm the localized carriers are in the 5d band. Bulk Au has an extremely low density of states and becomes diamagnetic, as is also the case for bare Au nanoparticles. This observation suggested that modification of the d band structure by chemical bonding can induce ferromagnetic like character in metallic clusters.

The first discovered nanomaterials was prepared by vacuum evaporation of iron in inert gas and condensed in cooled substrates [52]**.** After then many methods to fabricate nanoparticles including inorganic ceramics and organic compound are developed, such as arc plasma torch to produce metallic powder [53]**,** laser induced chemical vapor deposition method (CVDM) to produce special compounds [54], and microwave plasma enhanced CVD to produce hard and brittle materials. Instead of chemical vapor, the liquid co-precipitation can produce single-phase compounds [55] and the solid-state thermal decomposition can produce single-phase oxide metals [56] Some specified methods are illustrated.

(2.17) Metallic Nanoparticles

Various methods in preparation metallic nanoparticles invoke different properties with desired purposes. The widely exploited methods are:

The sol–gel method [57] Silver nanoparticles, for example, is prepared by mixing the AgNO3 solution with tetraethylorthosilicate(Si(OC2H5)4, TEOS), ethanol and water then with a few

drops of HNO3 as a catalyst. The mixed solution was dispersed and dried. The dried gels were reduced at a temperature of 400C for 30 min in hydrogen gas. The Ag particleshave a size of about 5∼10 nm with a profile distribution in the form of lognormal distribution.

The nanoparticles are embedded in silica glass in wellseparatedand protected matrix. The preparation of iron nanoparticles embedded in glass can be prepared with the same method by substituting FeCl3 for the silver salt [58,59]. The sol–gel method has advantages of yielding high purity, isotropic, and low temperature annealing while with shortage of cracking after dried by heavy doping. The free water absorbed in the porous gel and the H-O· bonds desorbed on the porous surface or the chemical absorbed hydroxyl groups which affects the optical absorption within the wavelengths of 160∼4500 nm can be removed by high temperature sintering. Hydrosol/magnetic fluid method: The pure metallic suspension particles such as noble metals can be prepared by hydrosol method by using reducing agent to embed in protective gelatin [60]**.** The advantage of the hydrosol method is that relatively narrow size distribution with average diameter of 20 can be achieved. The magnetic fluid with Fe3O4particles surrounded by oleic acid as surfactant for protection from their aggregation and dispersed in water can be prepared as described in Refs. [61, 62]**.**Vacuum deposition method: The presence of inert gas in vacuum chamber and lowering down the substrate temperature to liquid nitrogen temperature during thermal evaporation can reduce the momentum of the evaporated metallic atoms or clusters by collision with gas to obviate their further aggregation on the substrate. The evaporated metal atoms condensed just at where they reached without migration to the potential minimum thereby lose Vander attraction between particles. The resulting smokes can be collected from the substrate or walls of the evaporation chamber with the particle sizes can be easily controlled between 301000 depending on the gas pressure, the evaporation speed, the type of gas used, and the substrate temperature [63,64]**.** Direct (DC) or radio frequency (RF) sputtering with the structure of deposited films mostly to be amorphous without substrate heating can successfully deposit refractory metals and alloys. Ball milling method: Hard and brittle ceramic materials can be ball-milled into nanoparticles to produce nanocrytals, noncrystals, and pseudocrystals. Powders of 500 nm sizes can be milled into several nm by strong vibrations when mixed with tungsten-carbide (WC) spheres. The shortagesof ball milling are the surface contamination of the products and nonuniformity of the structure but is a simple method. Sometimes an addition of 1∼2% of methanol or phenol can prevent diffusion and solid reaction of the nanoparticles.

(2.18) Physical Properties of ATO Nanostructures

Transparent conducting oxide (TCO) films are widely used in a variety of optoelectronic devices such as solar cells, displays, and electrochromic devices. In recent years, there has been a growing interest in the application of TCO films as electrodes in solar cell devices. Among the TCO films, the most appropriate material for the application seems to be tin oxide films, which are chemically inert, mechanically hard, and heat resistant. In addition, they exhibit low electrical resistivity and high optical transmittance. Either doped or non-doped, tin oxide thin films can be fabricated by a number of techniques: chemical vapor deposition sputtering [65], sol-gel coating [66], and spray pyrolysis [67,68]. The sol-gel method has such advantages as cheap cost and flexible deposition technique. Such properties can be improved by doping tin oxide with, for example, antimony (Sb), indium (In), or fluorine (F). In fact, by increasing the doping concentration (>2%), a degenerate semiconductor is formed, displaying higher σ values (>103 Ω^{-1} cm^{-1}). Since this doping level is not too high, doped SnO_2 thin films are transparent for visible light, which makes them useful for a device application point of view. Also, the nature, quantity, and structural distribution of doping are important factors for the electrical properties of SnO_2 [69]. The current study investigates the characteristics of Sb-doped SnO_2 thin films prepared by dip coating technique. The structural, electrical, and optical properties of the thin films are examined in relation to the increase in the antimony amount.

(2.19) Structural Properties of ATO

antimony incorporation in SnO_2 lattice has not affected the structural properties to a considerable extent. On the other hand, for higher dopant levels, the incorporation would take place at interstitial sites, and some precipitation like antimony oxides (Sb_2O_3, Sb_2O_4, and Sb_2O_5) could be induced [70].As a result, with the increase of doping concentration, the deposited films lose the crystallinity, and the preferred orientation growth of SnO_2films may be suppressed by the precipitation. In the present case, antimony incorporation in SnO_2 lattice has not affected the structural properties to a considerable extent. It is also clear that , the crystallinity improves initially with antimony doping up to 7 at.% in the present case, but it decreases progressively beyond 7 at % doping concentration, as observed by Shanthi et al. [71].

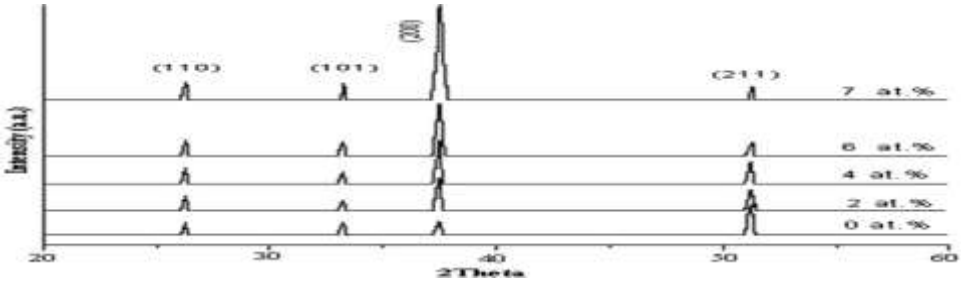

Figure (2.)10 XRD patterns of sol-gel ATO thin films deposited at550°C as function of Sb doping concentration .

(2.20) electrical properties of ATO

The effect of doping on the electrical properties of ATO thin films has been investigated. the variation of the resistivity (ρ) with different Sb doping concentration (atomic percentage). The resistivity of ATO thin films decreases initially with an increase in the Sb doping concentration to about 4×10^{-4} Ω cm for 2 at.% of Sb but increases again for further doping. The observed minimum is significantly less than that for pure SnO_2 thin films (5.4×10^{-3} Ω cm). The decrease in resistivity which may be attributed to the substitution of Sn^{4+} by Sb^{5+} [71], as their ionic radii match (Sn^{4+} 0.071 nm and Sb^{5+} 0.065 nm). The variation in the resistivity of tin oxide thin films with antimony doping is explained on the basis of the presence of Sb in two oxidations states, namely Sb^{5+} and Sb^{3+}. The possible mechanism may be as follo When SnO_2 is doped with Sb, a part of the lattice Sn^{4+} atoms are replaced bySb^{5+} resulting in the generation of conduction electrons and thus the decrease of resistivity [72,73]. Hence, a continuous decrease of resistivity is observed until Sb doping concentration ≤ 2 at.%. Beyond 2 at.% of Sb, the resistivity increases again. This is because beyond 2 at.% of Sb doping, a part of Sb^{5+} ions reduces to the Sb^{3+} state, resulting in the formation of acceptor sites and concomitant loss carriers [74,75]. The reduction of $Sb^{5+}$to Sb^{3+} has been verified by Terrier et al. by estimation of the lattice parameter of the doped SnO_2 films. Since the ionic radius of Sn^{4+} is less than that of Sn^{3+} but higher than that of Sn^{5+}, an increase in the lattice parameter of SnO_2 phase is observed beyond 2 at.% of Sb doping. This reduction of Sb^{5+} toSb^{3+} can be attributed to the increase in the resistivity above an optimum level of Sb doping.It is observed that this substitution increases the carrier concentration and thereby decreases resistivity. Thus, we could obtain the thin films which have the lowest resistivity at 2 at.% Sb doping level. The resistivity ρ is proportional to the reciprocal of the product of carrier concentration n and Hall mobility μ, as in the following equation:

$$\rho = \frac{1}{ne\mu} \qquad (2.64)$$

As Hall mobility decreased from 0.9024 to 0.2901 cm^2/Vs with Sb doping. The increase in Hall mobility may be attributed to the (1) increase in the addition of antimony at the tin site and (2) a decrease in grain boundary scattering. It is known that grain boundary scattering and ionized impurity scattering are two major scattering mechanisms determining the mobility variation of such extrinsic doped semiconductors. The resultant mobility is given as follows:

$$\frac{1}{\mu} = \frac{1}{\mu_{gb}} + \frac{1}{\mu_{is}} \qquad (2.65)$$

where μ is the resultant mobility; μgb is the mobility due to grain boundary scattering; and μis is the mobility due to ionized impurity scattering. These observations are in close coincidence with those of Shanthi [71], Agashe [76], and Advani [77]. the carrier concentration of thin films with an increase in Sb doping concentration. The substitution of Sn^{4+} by Sn^{5+} led to an increase in the carrier concentration because the radii of the two ions matched. The carrier concentration of the SnO_2 in films was 2.004 $\times 10^{19} cm^{-3}$ and the value increased continuously with Sb doping to 6 $\times 10^{19} cm^{-3}$ at 8 at.% Sb doping concentration

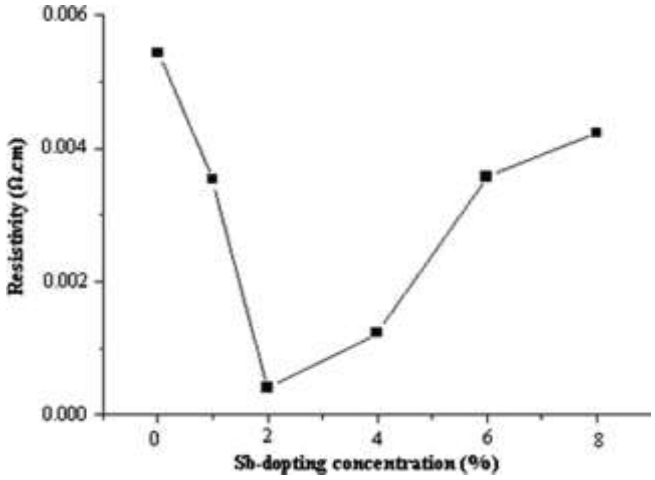

Figure (.2 . 11) Resistivity of ATO thin films with Sb doping concentration.

(2.21) Optical properties of ATO

The effect of doping on the optical properties of ATO thin films has been investigated. the transmittance spectra of ATO thin films with a thickness of 220 nm in the range of 300 to 2,000

nm. Maximum transmittance is found to be 96% (at 502 nm) for the ATO film doped with 2 at.% of Sb, which is attributed to the low scattering effect and thickness uniformity of the film due to surface smoothness of the film. However, the transmittance is found to decrease gradually if the antimony concentration is increased above 2 at.%. The decrease in transmittance with the increase in dopant concentration may be attributed to the increase in cluster size and surface roughness of the film, which promotes the diffuse and multiple reflections at the surface and increases the absorption. These observations are well in agreement with the results illustrated by Advani et al. and Manifacier [78,79]**,** Jarzebski [80], Ambrazeviciene [81]**,** and Shanthi**].** In the case of heavily doped semiconductors with carrier concentration being approximately 10^{19} to $10^{21}\mathrm{cm}^{-3}$, the Drude model can be generally used to represent the decrease in the transmittance [82]**.** Briefly, the model indicates that the transmittance drop in the near infrared region is associated with the plasma frequency (ωp) that can be expressed as follows:

$$\omega_p = \left[\frac{ne^2}{\varepsilon_0 \varepsilon_\infty m^*}\right]^{1/2} \qquad (2.65)$$

where n is the carrier concentration; e, the electronic charge; ε_0, the permittivity of free space; ε_∞, the high-frequency permittivity; m*, the conductivity effective mass. Below the plasma frequency, the films are characterized by a high reflectance, which functions as a screen of the incident electromagnetic wave. As ωp is proportional to the square root of the carrier concentration, the increase in the carrier concentration led to the lowering of the transmittance level near the infrared region

.

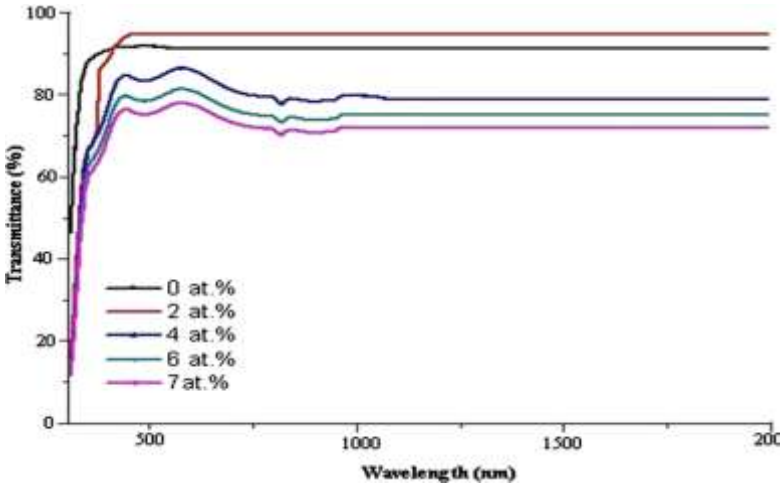

Figure.(2-12) Optical transmissions of undoped SnO_2 and several Sb-doped SnO_2 thin films as a wavelength function.

(2-22) Previous studies

(2.22.1) Microwave-assisted Fe-doped ZnO nanoparticles for enhancement of silicon solar cell efficiency

(In 2019) Ganga R. Neupanea, AmritKaphlea, ParameswarHaria,b,*

We have investigated the performance of a silicon solar cell coated with ZnO nanoparticle layers doped with ironvarying from (0–20%). We synthesized nanoparticles using a microwave method and fabricated thin film layerson silicon solar cells through a spin coating technique. The structure and morphology of nanoparticles wereanalyzed through transmission electron microscopy (TEM) and X-ray diffraction spectroscopy (XRD). The size ofthe particles decreased as iron concentration increased from 0 to 15%. Optical properties were analyzed through photoluminescence (PL) and absorption spectroscopy. PL spectra show a blueshift in the near band edgeemission peaks for 0–15% doped samples and a redshift for the 20% doped sample. The band gap of Fe–ZnOnanoparticles (0–15%) was found to increase from 3.20 eV to 3.24 eV, and the bandgap decreased to 3.22 eV for20% Fe–ZnO nanoparticles. Current-Voltage measurements confirm the enhancement in power conversion efficiency by 30% with iron doping in ZnO up to 15%. Efficiency increased with nanoparticle layers up to180.29 nm in every sample and decreased with further increase in thickness. Enhancement in external quantumefficiency (EQE) was also observed with the increase in dopant concentration up to 15%. The optimum thicknessof the ZnO nanoparticle layer was found to be approximately 180 nm for maximum enhancement in conversionefficiency[83]

(2.22.2)Enhanced solar cell performance of P3HT:PCBM by SnS nanoparticles

(In 2020) SeyedehLalehMousavia, FaridJamali-Sheinib,, Mohammad Sabaeianc,d, RaminYousefie

In this research, un- and zinc (Zn)-doped tin sulfide (SnS) nanoparticles (NPs) were synthesized by ultrasoundmethod and added to the active layer of ITO/PEDOT:PSS/P3HT: PCBM/Al polymer solar cells (PSCs). Thestructural, optical, and electrical properties due to the influence of NPs on solar cell performance were investigated. The X-ray diffraction (XRD) patterns of the NPs indicates the formation of orthorhombic polycrystalline SnS. Field emission scanning electron microscopy (FESEM) images show spherical particles with sizeless than 100 nm for un- and Zn-doped SnS samples. Optical analysis of the cells shows a decrease in the bandgap due to the presence of un- and Zn-doped SnS NPs. Photovoltaic characterization of the samples shows

that byadding NPs to the polymer film, the device performance improves significantly compared to the absence of NPs.The presence of NPs with different concentrations and structural defects affects the electro-optical properties ofthes[84]

(2.22.3) Engineering aluminum oxide/polysilicon hole selective passivated contacts for high efficiency solar celq

(nI2020) Gurleen Kaur a,b,*, Zheng Xin b, RanjaniSridharan b, Aaron Danner a,b, Rolf Stangl b

Tunnel layer passivated contact technology is already highly efficient in case of selective electron extraction butnot as efficient in case of selective hole extraction. Thus far, SiOx/p+-poly-Si contacts have resulted only in efficiencies above ~20.1% for rear-side deployed hole selective contacts. We investigate if hole extraction selectivity can be further improved by substituting the 'conventionally' used SiOx tunnel layer exhibiting moderate oreven high positive fixed charge density by AlOx tunnel layers, exhibiting high negative fixed charge density. Themerits of using atomic layer deposited ultrathin AlOx tunnel layers are investigated and compared with wetchemically formed SiOx tunnel layers to form AlOx/p+-poly-Si and SiOx/p+-poly-Si hole selective passivatedcontacts respectively. The AlOx thickness (0.13–2 nm) and its thermal budget including annealing time, temperature and ambient were varied. The quality of the resulting AlOx/p+-poly-Si passivated contacts was determined by measuring the recombination current density (Jc) and the effective contact resistivity (ρc). Finally,using the measured values of Jc and ρc, we predict the efficiency potential and selectivity of the passivatedcontact using Brendel's model. We show that for 425 ◦C annealed AlOx samples prior to poly-Si capping, there isan improvement in passivation quality due to the high negative AlOx interface charge, which forms only for"thick" tunnel layers (≥1.5 nm). However, after high-temperature poly-Si capping, enhanced boron in-diffusionand charge compensation are degrading the overall passivation quality of "thick" AlOx/p+-poly-Sipassivatedcontacts. The best AlOx/p+-poly-Si passivated contacts use ultra-thin AlOx tunnel layers (efficiency potential of26.9%), which is only marginally better than the SiOx reference samples, but still improves hole selectivity.[85]

(2.22.4) Progress in plasmonic solar cell efficiency improvement: A statusreview

(In 2016) P. Mandal n, S. Sharma

Solar cell efficiency improvement has been one of the major concerns to realize ultimately thecosteffective efficient solar cells. Among various ways to improve solar cell efficiency,

plasmonic lighttrapping mechanism has been found to be of immense interests recently. The mechanism of strongscattering into the active materials and guiding of light at the excitation of plasmons at the metalsemiconductor interface play significant role for better photon harvesting. The present review concentrates on the recent advances on the application of plasmonics in inorganic semiconductor solar cellefficiency improvements. Various research groups active in this field have employed various metal nanostructures on to the surface of solar cells to achieve higher efficiency. This review partially also concentrates on surface nanopatterning of solar cells with nonmetallic dielectrics. Finally, a brief account onthe dye-sensitized solar cell is presented to show the potential of plasmonics in solar cell research[86]-

(2.22.5) Theoretical investigation of broadband absorption enhancement in a-Sithin-film solar cell with nanoparticles

(In 2020) Hongen Li , Yizhi Hu , Yue Yang *, Yonggang Zhu

Thin-film solar cells have attracted increasing attention due to its low material cost and large flexibility, but theyalso face the challenge of low solar absorption due to reduced active layer thickness. Through exciting surfaceplasmon resonance, plasmonic metal nanoparticles are usually placed on the cell front surface to enhance solarabsorption. However, if eliminating the unuseful intrinsic absorption in nanoparticles, we find that dielectricones are better choices to enhance a-Si thin-film solar cell absorption efficiency. Moreover, a composite lighttrapping structure with dielectric nanoparticles on the front surface and metal hemispheres on the rear surface isproposed to achieve broadband absorption enhancement in both short and long wavelengths, with the aim to geta higher conversion efficiency. The finite-difference-time-domain simulation results show that, compared withbare 100-nm-thick amorphous silicon solar cell, the short-circuit current density and photoelectric conversionefficiency could berespectively improved by 21% and 18% with addition of optimized composite light trappingstructure. The general method proposed in this study could provide valuable guidance to light trapping structuredesign for various kinds of thin-film solar cells. [87]-

(2.22.6) Fe-doped Graphene Nano sheet as an Adsorption Platform of Harmful Gas Molecules (CO, CO2, SO2 and H2S), and the co-adsorption in O2environments

(in24-8-2017) Diego Cortes-Arriagada, Nery Villegas-Escobar, ´ Daniela E. Ortega

The adsorption of pollutant gases (CO, CO2, SO2 and H2S) onto Fe-doped graphene nanosheets (FeG) is studied on the basis of density functional theory calculations at the PBE/Def2-SVP level

of theory. The most stable adsorption configurations, binding Gas−characteristics, electronic properties and stability at room temperature of the FeG interactions is fully analyzed. The gas molecules are chemisorbed onto FeG with adsorption energies in the range of 0.54 to 1.8 eV, with an enhanced adsorption strength compared to intrinsic graphene. The stability of the FeG-Gas interactions is dominated by Lewis-acidbase interactions, and its strength is sorted as SO2>CO>H2S>CO2. The adsorption stability is also retained at room temperature (300 K). Due to the strong interaction of SO2, CO, and H2S, FeG could catalyze or activate these gas molecules, suggesting the possibility of FeG as a catalyst substrate. The electron acceptor/donor character of CO, CO2, SO2 and H2S molecules when adsorbed onto FeG causes charge transfer processes that are responsible for the change in conductance of FeG; thus, the response of the HOMO-LUMO gap of FeG under gas adsorption could be useful for sensing applications. Furthermore, the analysis of the co-adsorption in O2 environments shows that the CO2 interaction turns unstable onto FeG, while the sensing response towards H2S is suppressed. Finally, these results give new insights into the emerging applications of Fe-doped graphene in gas capture/filtration devices, solid-state gas sensors or as a catalyst substrate. [88]-

(2.22.7) Engineering aluminum oxide/poly silicon hole selective passivated contacts Anodic Aluminum Oxide Passivation For Silicon Solar Cells

(In JANUARY 2013) P. H. Lu, K. Wang, Z. Lu, A. J. Lennon, and S. R. Wenham, Member, IEEE

The requirement to form localized rear metal contactregions for higher silicon solar cell efficiencies places demand onpatterning techniques in terms of the small size of the openings andthe ability to perform the patterning at commercial wafer processing rates. We suggest here the possibility of using a self-patterning approach which offers the potential of enhanced surface passivation and nanoscale patterning achieved using a single electrochemical anodization process. It is shown that when nonporous anodic aluminum oxide (AAO) layers are formed by anodizing an aluminum layer over an intervening SiO2 or SiNx dielectric layer,the implied open-circuit voltages of p-type silicon test structurescan be increased by an average of 40 and 47 mV, respectively. Capacitance–voltage measurements show that these passivatingAAO dielectric stack layers store positive charges, which differsfrom what is observed for Al2 O3 layers deposited by plasma enhanced chemical vapor deposition or atomic layer deposition. Furthermore, we show that the magnitude of the stored charge inthe dielectric stacks depends on

the anodization conditions, highlighting the possibility of controlling the charge storagepropertiesof these layers for specific cell requirements. Although the passivating properties of the anodized aluminum layer appear to bestrongly influenced by charge effects, it is also possible that hydrogenation effects may play a role as has been previously observedfor other electrochemical processes, such as metal plating[89]-

(2.22.8) Enhancement of dye sensitized solar cell efficiency through introducing concurrent up conversion/down conversion core/shell nanoparticles as spectral converters

(In 2018) Tong Chen a, Yunfei Shang a, ShuweiHao a, b, *, Li Tian a, YuedanHou a,Chunhui Yang a

Extending the spectral absorption of dye-sensitized solar cells from the visible into near-infrared andultra-violet range enables the minimization of non-absorption loss of solar photons. Here, we report aviable strategy to implement simultaneously near-infrared up conversion and ultra-violet down conversion for dye-sensitized solar cells through constructing a type of up conversion-core/ down conversion – shell - structured nanoparticles. For the first time, NaYF4:20%Yb,2%Er@NaYF4:7%Eucore/shell nanoparticles are applied to TiO2 photoanode for fabricating near-infrared/ultra-violet-enableddye-sensitized solar cell devices. Theincorporation of designed nanoparticles into TiO2 photoanode ofdye-sensitized solar cells achieves high efficiency of 7.664% under one sun illumination, increasing thepower conversion efficiency by about 13.95%. We confirm that the enhancement of overallefficiencyincludes 4.82% upconversion contribution, 7.58% down conversion function and 1.55% scattering effect.Our strategy opens the path for further broadening the solar spectral use to improve the performance ofphotovoltaic devices.[90]-

(2.22.9) Aggrandize efficiency of ultra-thin silicon solar cell via topical clustering of silver nanoparticles

(In 2018) T. Thirugnanasambandan a, K. Pal b,*, Sidhu A. c, M. AbdElkodous d, H. Prasath e,K. Kulasekarapandian f, A. Ayeshamariam g, J. Jeevanandam h

A highly efficient photovoltaic nanocomposite device is demonstrated by fabrication of structural clustersof silver nanoparticles (Ag NPs) on silicon solar cells via a boil deposition method. The efficiency of siliconsolar cell was augmented by coating Ag NPs ultra-thin-film deposition on silicon solar cell. Chemically synthesized silver NP’s, their consumption on a silicon thin layer and the operation of photovoltaicnanocomposite device were characterized by

using several electron probe microscopic pectroscopic and spectrometric techniques viz. x-ray diffraction (XRD), scanning electron microscopy (SEM), highresolution transmission electron microscopy (HR-TEM), Photoluminescence, UV–visible absorption, dielectric, current vs. voltage (I ~ V) and capacitance vs. voltage (C ~ V)characteristics. Poly-dispersednature of 'Ag' nanoparticles established the anisotropy of these NPs when coated on silicon solar cells.Their efficiency enhancement was confirmed from HR-TEM image via time-domain finitedifferencetechnique to deliberate the particle distribution effect on an ultra-thin film of silicon solar cell, indicating[91]-

(2.22.10) Nanoparticle-Tuned Self-Organizationof a Bulk Heterojunction Hybrid SolarCell with Enhanced Performance

(In2012) Hsueh-Chung Liao,† Cheng-Si Tsao,‡,* Tsung-Han Lin,† Meng-HuanJao,† Chih-Min Chuang,‡ Sheng-Yong Chang,§ Yu-Ching Huang,‡ Yu-Tsun Shao,§ Charn-Ying Chen,‡ Chun-Jen Su,^ U-SerJeng,^Yang-Fang Chen,§ and Wei-Fang Su†,*

We demonstrate here that the nanostructure of poly(3-hexylthiophene) and phenyl-C61-butyricacid methyl ester (P3HT/PCBM) bulk heterojunction (BHJ) can be tuned by inorganic nanoparticles(INPs) for enhanced solar cell performance. The self-organized nanostructural evolution of P3HT/PCBM/INPs thin films was investigated by using simultaneous grazing-incidence small-angle X-rayscattering (GISAXS) and grazing-incidence wide-angle X-ray scattering (GIWAXS) technique. IncludingINPs into P3HT/PCBM leads to (1) diffusion of PCBM molecules into aggregated PCBM clusters and (2)formation of interpenetrating networks that contain INPs which interact with amorphous P3HTpolymer chains that are intercalated with PCBM molecules. Both of the nanostructures provideefficient pathways for free electron transport. The distinctive INP-tuned nanostructures are thermallystable and exhibit significantly enhanced electron mobility, external quantum efficiency, andphotovoltaic device performance. These gains over conventional P3HT/PCBM directly result fromnewly demonstrated nanostructure. This work provides an attractive strategy for manipulating thephase-separated BHJ layers and also increases insight into nanostructural evolution when INPs areincorporated into BHJs. [92]-

Chapter Three

Materials and Experimental Method

(3.1) Introduction

This chapter is concerned with the experimental work. Which includes Materials, sample preparation and techniques uses .In this work ten samples of five samples ($Ni_x\ Al_{2(1-x)}O_4$)and five samples ($Ni_x\ S_{1-x}\ O_4$) were prepared.

(3.2) Materials

(3.2.1) Aluminum nitrate ($Al_{2(1-X)}\ O_4$)

($Al_{2(1-X)}\ O_4$) is a white, water-soluble salt of aluminum and nitric acid, most commonly existing as the crystalline hydrate, aluminum nitrate Nona hydrate, Al(NO3)3·9H2O.

(3.2.1.1) Properties

Chemical formula Al(NO4)Molar mass 212.996 g/mol (anhydrous) 375.134 g/mol (Nona hydrate) Appearance White crystals, solid hygroscopic Density 1.72 g/cm3 (Nona hydrate Melting point 66 °C (151 °F; 339 K) (anhydrous)[1] 73.9 °C (165.0 °F; 347.0 K) (nonahydrate Boiling point 150 °C (302 °F; 423 K) (Nona hydrate) decompose Refractive index (nD) 1.54 [93,94]

(3.3) Nickel nitrate

Is the inorganic compound Ni (NO3)2 or any hydrate thereof. The anhydrous form is not commonly encountered, thus "nickel nitrate" usually refers to nickel (II) nitrate hexahydrate. The formula for this species is written in two ways: Ni (NO3)2.6H2O and, more descriptively [Ni (H2O)6] (NO3)2. The latter formula indicates that the nickel (II) center is surrounded by six water molecules in this hydrated salt. In the hexahydrate, the nitrate anions are not bonded to nickel. Also known are three other hydrates: Ni(NO3)2.9H2O, Ni(NO3)2.4H2O,and Ni(NO3)2.2H2O. Anhydrous Ni(NO3)2 is also known[95]

(3.3. 1) Properties

Chemical formula Ni(NO3)2 ,Molar mass182.703g/mol,(anhydrous) 290.79 g/mol (hexahydrate Appearance emerald green hygroscopic solid,Density 2.05 g/cm3 (hexahydrate),Melting point 56.7 °C (134.1 °F; 329.8 K) (hexahydrate),Refractive index(nD)1.422 (hexahydrate) [96,97 98].

(3.4) Nitric Acid

Molecular formula HNO_3 , molar mass 63.012 g/mole, Physical state (liquid), Color: Colorless, melting point -42°C, density 1.5129g/cm³ °C, Solubility. Completely miscible.

(3.5) Distilled Water

Distilled water is steam from boiling water that's been cooled and returned to its liquid state. It's the purest water.3.3 Synthesis of ($Ni_x Al_{2(1-x)}O_4$) and ($Ni_x S_{1-x} O_2$) Nano Powder fabricated , 5 from $Ni_x Al_{2(1-}x)O_4$ with (X =0.1 , 0.3 , 0.5 , 0.7 , 0.9) and 5 from Ni $xS_{1-x} O_2$assuming the same values for x. The firstly synthesis 5 from $Ni_x Al_{2(1-x)}O_4$with (X =0.1 , 0.3 , 0.5 , 0.7 , 0.9) by the sol-gel method. aluminum nitrate ($AL_{2\ (1-x)}\ O_4$)) , were used as starting material, distilled water as dissolving medium and nitric acid as adjusting of PH less than 5 PH . . Then the solution was stirred and heated after PH was adjusted to 5.0 at80c0 for one hour.

Table (3-1) aluminum nitrate ($Ni_x\ AL_{2\ (1-x)}\ O_4$)

Test 1	M	mass	Distend water
Ni_x	0,1	29.08	2.89
$Al_{2(1-x)}$	0.9	337.62	26.08
Test2			
Ni_x	0.3	87.24	8.69
$Al_{2(1-x)}$	0.7	262.59	20.29
Test3			
Ni_x	0.5	145.39	14.49
$Al_{2(1-x)}$	0.5	187.57	20.29
Test4			
Ni_x	0.7	203.56	20.29
$Al_{2(1-x)}$	0.3	112.54	8.96
Test5			
Ni_x	0.9	29.08	2.89
$Al_{2(1-x)}$	0.1	37.51	2.89

The secondly synthesis 5 from $Ni_x\ S_{1-x}\ O_4$ with (X = 0.1, 0.3, 0.5, 0.7, 0.9) by the sol- gel method were used $Ni_x\ S_{1-x}\ O_4$ as starting material, distilled water as dissolving medium and nitric acid as adjusting of PH less than 5 PH . Then the solution was stirred and heated after PH was adjusted to 5.0 at80c_0 for one hour.

Table (3-2) aluminum nitrate ($Ni_x S_{1-x}O_4$)

Test 1	M	mass	Disteld water
Ni_x	0,1	29.08	2.89
$S_{1-x}O_4$	0.9	68.51	26.08
Test2			
Ni_x	0.3	87.24	8.69
$S_{1-x}O_4$	0.7	53.29	20.29
Test3			
Ni_x	0.5	145.39	14.49
$S_{1-x}O_4$	0.5	38.06	14.49
Test4			
Ni_x	0.7	203.56	20.29
$S_{1-x}O_4$	0.3	22.84	8.69
Test5			
Ni_x	0.9	261.72	26.08
$S_{1-x}O_4$	0.1	7.61	2.89

The volume of water was determined by the molarity equation:

$$M_0 = \frac{n}{V_w \times 1000}$$

Since,

$$n = \frac{W_g}{W_m}$$

$$V_w = \frac{W_g}{M_0 \times 1000 \times W_m}$$

Where: n is number molar. M_0 is the molecular concentration

Vw is volume of water. Wg is weight by gram of sample

Wm is the molecular weight.

Secondly the two solutions were mixed and added 3.0g of titanium oxide, the product mixture was heated and stirred at 80c0 continuously about one hour, the last one was deposited for one day then filtered to obtain pure solution (Hydrolysis step), which was slowly evaporated to form

sol by continues in heat treatment convert to gel at150c0 after two hours (gelation step). Finally the gel was dried and grinded to powder.

(3.6) Techniques Uses

The structure of the samples was characterized by X-ray diffraction (XRD) and the optical properties were investigated by using UV-visible absorption spectrophotometer

(3.6.1) X-ray Diffractometer

X-ray diffraction is a common technique for study of crystal structures and atomic spacing. All X-ray diffractometers consist of three basic element: x –ray tube, a sample holder, and x- ray detector.

X- rays generated in cathode ray tube by heating filament to produce electrons, accelerating the electrons toward a target by applying a voltage, and bombarding the a target material with electrons. When electrons have sufficient energy to dislodge inner shell electrons of target material, characteristic x- ray spectra are produced. These spectra consist of several components, the most common beingk_{α} andk_{β}. k_{α} Consist in part of $k_{\alpha 1}$ and$k_{\alpha 2}$. $k_{\alpha 1}$has slightly shorter wavelength and twice the intensity as Kα2. The specific wavelengths are characteristic of the target material (Cu, Fe, Mo, Cr). Filtering, by foils or crystal monochrometers, is required to produce monochromatic X-rays needed for diffraction. Kα1and Kα2 are sufficiently close in wavelength such that a weighted average of the two is used. Copper is the most common target material for single-crystal diffraction, with Cu Kα radiation = 1.5418Å. These X-rays are collimated and directed onto the sample. As the sample and detector are rotated, the intensity of the reflected X-rays is recorded. When the geometry of the incident X-rays impinging the sample satisfies the Bragg Equation, constructive interference occurs and a peak in intensity occurs. A detector records and processes this X-ray signal and converts the signal to a count rate which is then output to a device such as a printer or computer monitor [99].

Figure (3-1) X-Ray diffract meter: XRD (wavelength 1.54 A°)

(3.6.2) FTIR Spectroscopy

FTIR spectroscopy is a widely used technique for investigating materials. It is based on the interaction electromagnetic radiation and natural vibration of chemical bonds among atoms that compose the matter.

The main components of FTIR spectroscopy are: IR source, Michelson interferometer and IR detector. The more stable source of radiation, emitting in the three IR regions is the Ever-Glo ceramic. By using the appropriate beam splitter (interferometer components) and IR detector in combination with this source, it is possible to provide energy for the spectral range from to. The Michelson interferometer basically consists of two perpendicularly plane mirrors (one is fixed and the other movable) and beam splitter. The function of an interferometer is split beam of light into two beams and to introduce an optical path difference between them. As a consequence, the path difference creates the condition for that interference to take place when the beams recombine at the beam splitter. The intensity vibrations of the beam emerging from the interferometer are monitored as function of path difference by the detector. The light intensity versus the optical path difference is called an interferogram. The Fourier-transform is mathematic tool used to convert the interferogram into spectrum, which is done by computer]. .

Figure (3-2) FTIR (Mattson, model 960m0016) spectroscopy.

(3.6.3) Ultraviolet -Visible Spectroscopy (UV-Visible)

Ultraviolet and Visible Spectroscopy is absorption spectroscopy uses electromagnetic radiations between 190 nm to 800 nm and is divided into the ultraviolet (UV, 190-400 nm) and visible (VIS, 400-800 nm) regions. Since the absorption of ultraviolet or visible radiation by a molecule leads transition among electronic energy levels of the molecule, it is also often called as electronic spectroscopy [106].When radiation interacts with matter, a number of processes can occur, including reflection, scattering, absorbance, Fluorescence/phosphorescence (absorption and reemission), and photochemical reaction (absorbance and bond breaking). In general, when measuring UV-visible spectra, we want only absorbance to occur. Because light is a form of energy, absorption of light by matter causes the energy content of the molecules (or atoms) to increase. The total potential energy of a molecule generally is represented as the sum of its electronic, vibrational, and rotational energies [107,].

The absorption spectra of prepared nanoparticles were measured using shimadzu spectrophotometer (UV mini 1240) in 190-800nm range see figure (3.3)

Figure (3-3): UV mini 1240 spectrometer shimadzu.

Chapter Four

Results, Discussion and conclusion

(4.1) Introduction

The results that have been obtained for ($Ni_{0.1}Al_{0.9}O_4$) samples are presented. The data of X-ray diffraction (XRD) have been analyzed using Riveted method for crystal structure, lattice parameters, the positions of atoms within the cell).The FT-IR data have been done to investigate the chemical bonds. The data of UV-visible can be used to for the band gap and absorption coefficient.

(4.2) XRD Result for NixAL2 (1-x)O4

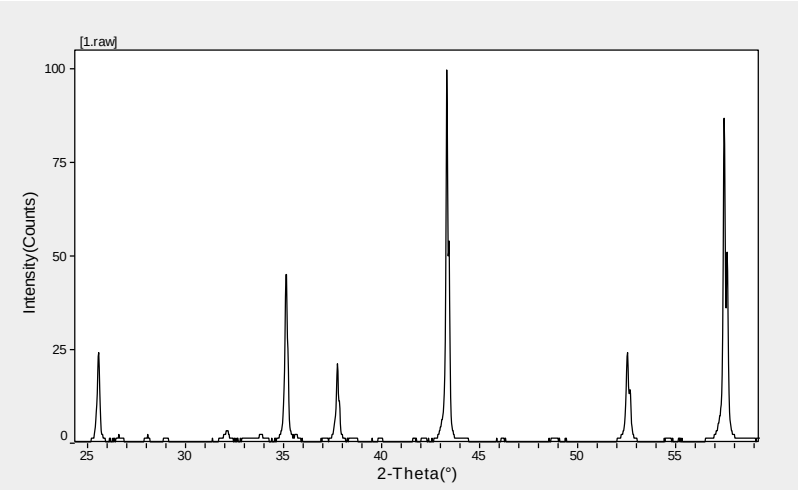

Figure (4.1) XRD spectrum of ($Ni_{0.1}Al_{0.8}O_4$)sample

Table (4.1) Lattice Constants from Peak Locations and Miller Indices [Orthorhombic A-Center] of ($Ni_{0.1}Al_{0.8}O_4$)sample

2Θ	d (nm)	h k l
25.572	3.41207	8 11
35.128	2.50096	1300
37.750	2.33318	2 33
43.330	2.04438	0 4 2
52.547	1.70559	5 4 4
57.477	1.56996	11 2 6

Average Lattice Constants = 32.7107

a=33.326 b= 8.869 c =12.499

$\alpha = \beta = \gamma = 90^{O}$

Density = 7.9037 mg.cm^{-3}

Crystal Form: Orthorhombic –A Center

Spacing Groups: Abm2 (39)

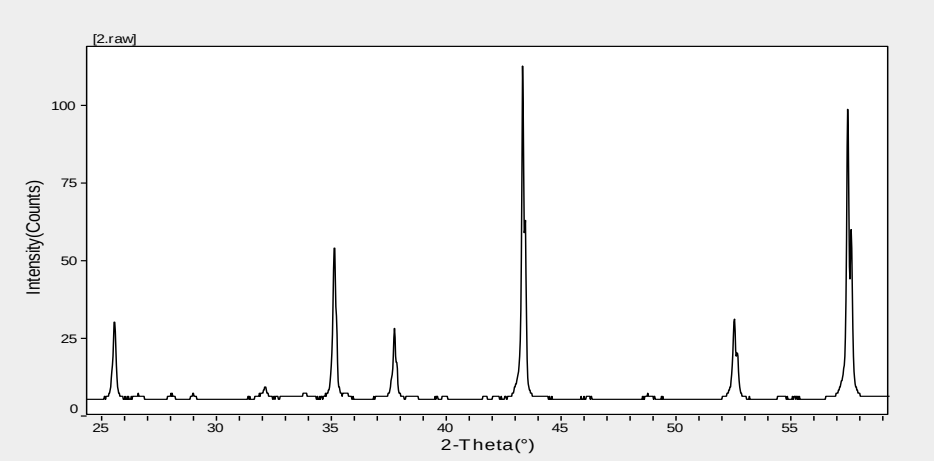

Figure (4.2) XRD spectrum of ($Ni_{0.3}Al_{1.4}O_4$)sample

Table (4.2) Lattice Constants from Peak Locations and Miller Indices [Orthorhombic A-Center] of ($Ni_{0.3}Al_{1.4}O_4$)sample

2Θ	d (nm)	h k l
25.572	3.4817	8 1 1
35.128	2.5520	13 0 0
37.750	2.3808	2 3 3
43.330	2.0861	0 4 2
52.547	1.7404	5 4 4
57.477	1.6020	11 2 6

Average Lattice Constants = 32.7109

a=33.326 b= 8.869 c =12.499

$\alpha = \beta = \gamma = 90^{O}$

Density = 7.74563mg.cm^{-3}

Crystal Form: Orthorhombic –A Center

Spacing Groups: Abm2 (39)

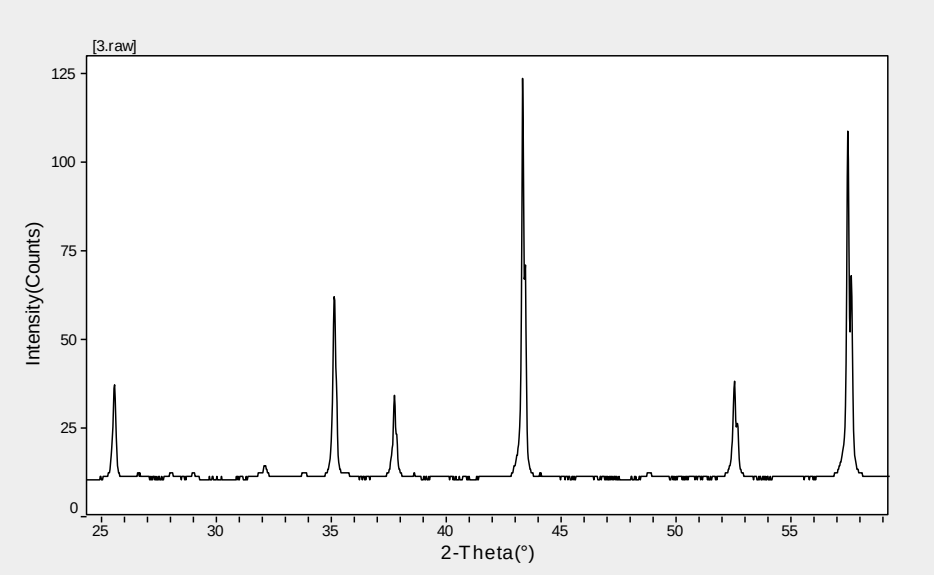

Figure (4.3) XRD spectrum of ($Ni_{0.5}Al_{0.1}O_4$)sample

Table (4.3) Lattice Constants from Peak Locations and Miller Indices [Orthorhombic A-Center] of ($Ni_{0.5}Al_{0.1}O_4$)sample

2Θ	d (nm)	h k l
25.572	3.41207	8 1 1
35.128	2.5009	13 0 0
37.750	2.3332	2 3 3
43.330	2.0444	0 4 2
52.547	1.7056	5 4 4
57.477	1.5699	11 2 6

Average Lattice Constants = 32.7111

a=33.326 b= 8.869 c =12.499

$\alpha = \beta = \gamma = 90^O$

Density = 7.59072mg.cm^{-3}

Crystal Form: Orthorhombic –A Center

Spacing Groups: Abm2 (39)

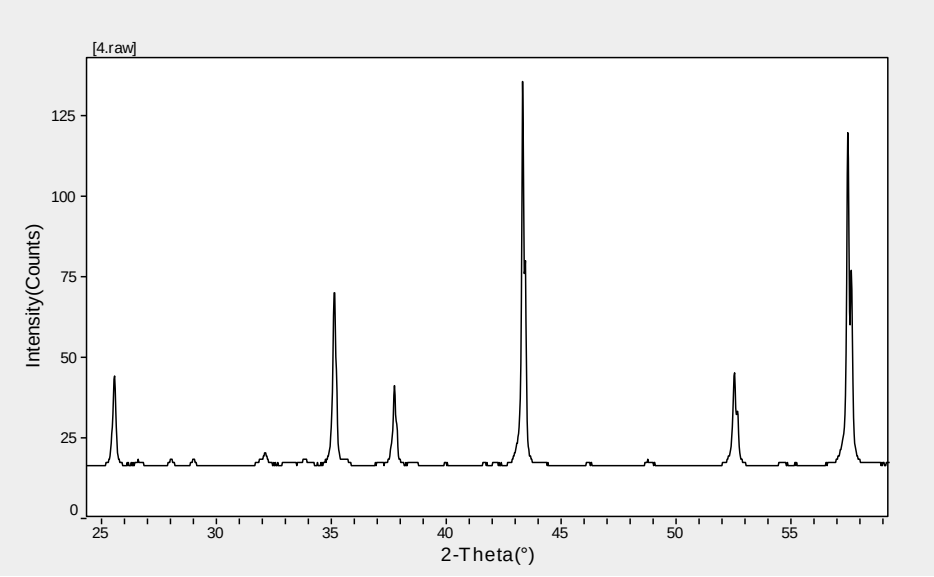

Figure (4.4) XRD spectrum of ($Ni_{0.7}Al_{0.6}O_4$)sample

Table (4.4) Lattice Constants from Peak Locations and Miller Indices [Orthorhombic A-Center] of ($Ni_{0.7}Al_{0.6}O_4$)sample

2Θ	d (nm)	h k l
25.572	3.3438	8 1 1
35.128	2.4509	13 0 0
37.750	2.2865	2 3 3
43.330	2.0032	0 4 2
52.547	1.6715	5 4 4
57.477	1.5385	11 2 6

Average Lattice Constants = 32.7113

a=33.326 b= 8.869 c =12.499

$\alpha = \beta = \gamma = 90^O$

Density = 7.43891mg.cm^{-3}

Crystal Form: Orthorhombic –A Center

Spacing Groups: Abm2 (39)

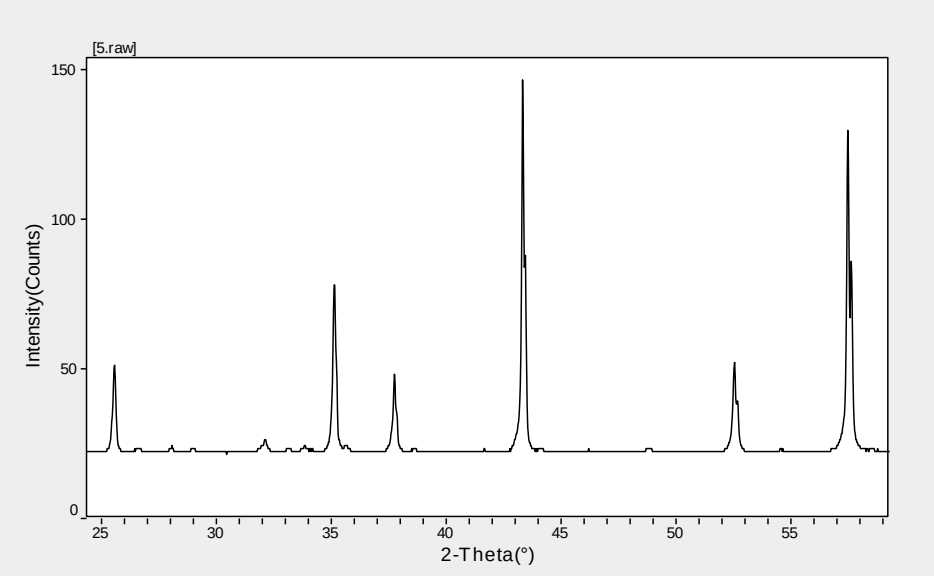

Figure (4.5) XRD spectrum of ($Ni_{0.9}Al_{0.2}O_4$)sample

Table (4.5) Lattice Constants from Peak Locations and Miller Indices [Orthorhombic A-Center] of ($Ni_{0.9}Al_{0.2}O_4$)sample

2Θ	d (nm)	h k l
25.572	3.2769	8 1 1
35.128	2.4019	13 0 0
37.750	2.2408	2 3 3
43.330	1.9631	0 4 2
52.547	1.6381	5 4 4
57.477	1.5077	11 2 6

Average Lattice Constants = 32.7116

a=33.326 b= 8.869 c =12.499

$\alpha = \beta = \gamma = 90^O$

Density = 7.29012mg.cm^{-3}

Crystal Form: Orthorhombic –A Center

Spacing Groups: Abm2 (39)

Table (4.6) some crystallite lattice parameter (c- form , a,b,c, β,α, γ, density ,Xs(nm) and d – spacing) of all samples that meade by ($Ni_x Al_{1-x} O_4$)

Sample	a	B	c	α= β γ	Density(g.cm^{-3})	d-spacing (A^o)
$Ni_{0.1} Al_{0.8} O_4$	33.326	8.869	12.499	90	7.9037	2.26102
$Ni_{0.3} Al_{0.4} O_4$	33.326	8.869	12.499	90	7.74563	2.30716
$Ni_{0.5} Al_{0.1} O_4$	33.326	8.869	12.499	90	7.59072	2.26101
$Ni_{0.7} Al_{0.6} O_4$	33.326	8.869	12.499	90	7.43891	2.21573

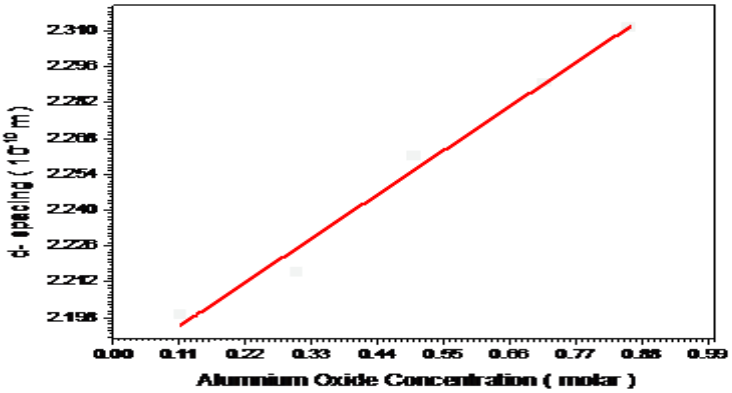

Figure (4.6) relationship between Al_{1-x} rated and d-spacing of all ($Ni_x Al_{1-x} O_4$)samples

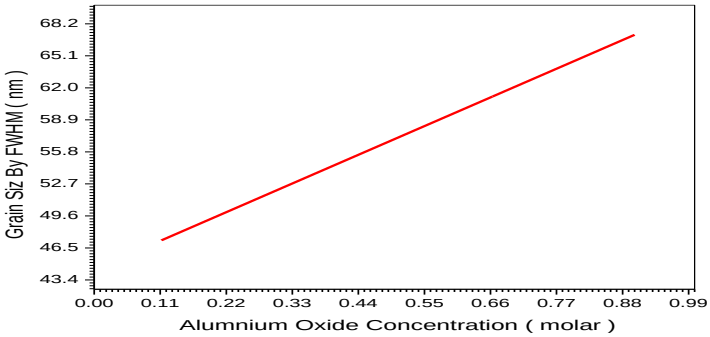

Figure (4.7) relationship between Al_{1-x} rated and crystallite size of all ($Ni_x Al_{1-x} O_4$)samples

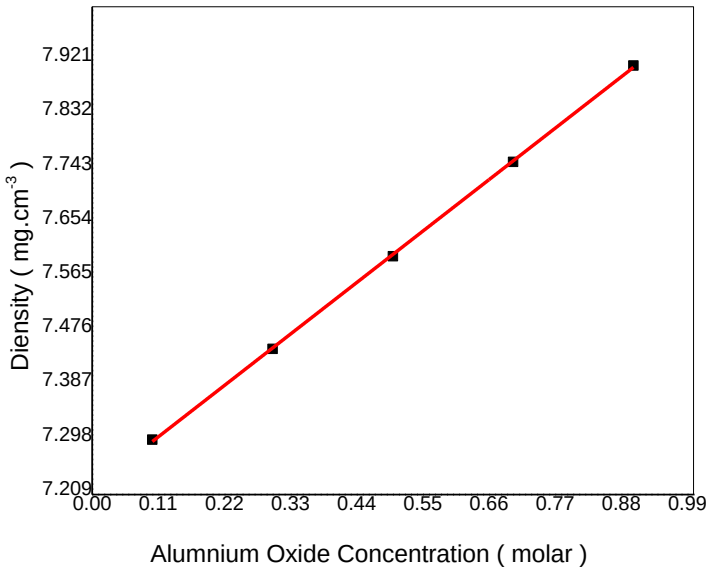

Figure (4.8) relationship between Al_{1-x} rated and Density of all ($Ni_x Al_{1-x} O4$)samples

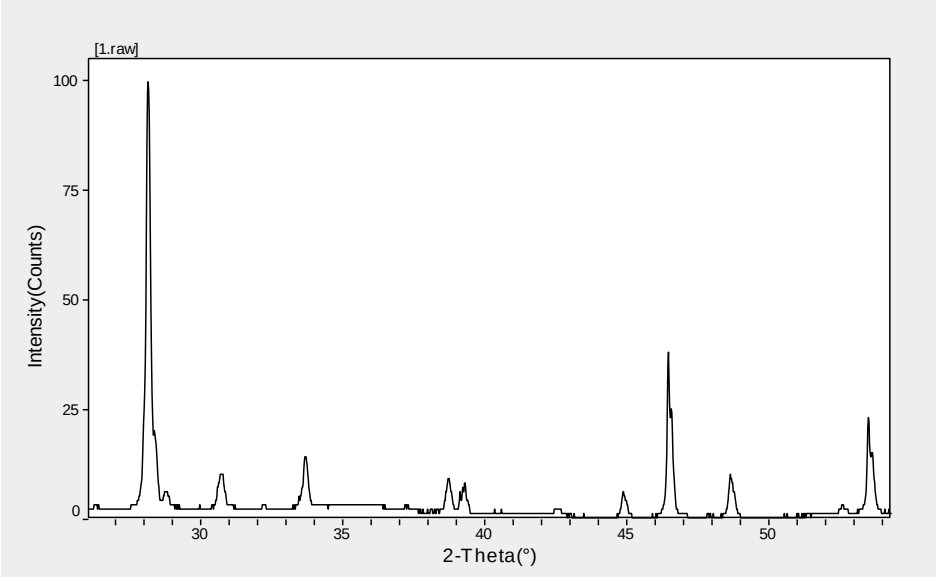

Figure (4.9) XRD spectrum of (Ni 0.1 S 0.9 O4)sample

(4.3) XRD result of $Ni_xS_{1-x}O_4$

Table (4.7) Lattice Constants from Peak Locations and Miller Indices [Orthorhombic A-Center] of ($Ni_{0.9}S_{0.1}O_4$) sample

2Θ	d (nm)	h k l
28.131	3.1695	2 1 2
46.469	1.9526	422
53.510	1.7110	2 3 3

Average Lattice Constants = 11.3483

a= 9.7984 b= 8.2759 c =9.6138

$\alpha = \beta = \gamma = 90^O$

Density = 1.9013mg.cm^{-3}

Crystal Form: Orthorhombic –A Center

Spacing Groups: Abm2 (39)

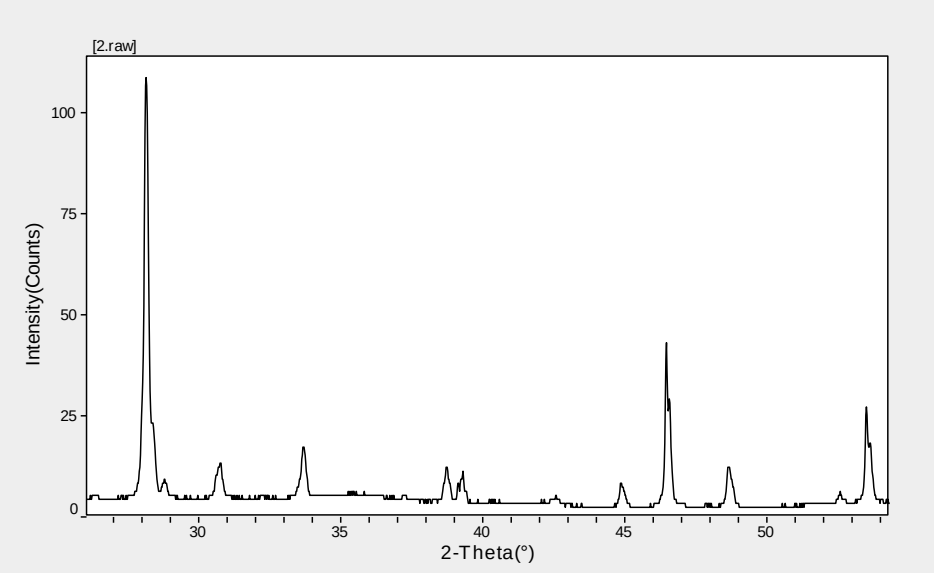

Figure (4.10) XRD spectrum of ($Ni_{0.9}S_{0.1}O_4$)sample

Table (4.8) Lattice Constants from Peak Locations and Miller Indices [Orthorhombic A-Center] of ($Ni_{0.7}S_{0.3}O4$) sample

2Θ	d (nm)	h k l
28.131	3.0115	2 1 2
46.469	1.9135	4 2 2
53.510	1.6768	2 3 3

Average Lattice Constants = 11.3481

a= 9.7984 b= 8.2759 c =9.6138

$\alpha = \beta = \gamma = 90^{O}$

Density = 1.9035 $mg.cm^{-3}$

Crystal Form: Orthorhombic –A Center

Spacing Groups: Abm2 (39)

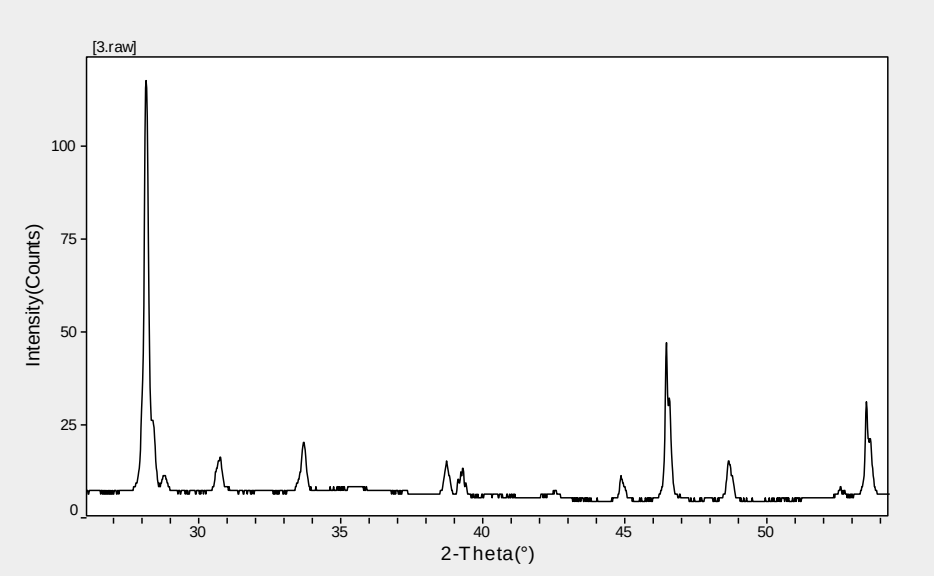

Figure (4.11) XRD spectrum of (Ni 0.7 S 0.3 O4) sample

Table (4.9) Lattice Constants from Peak Locations and Miller Indices [Orthorhombic A-Center] of ($Ni_{0.5}S_{0.5}O_4$) sample

2Θ	d (nm)	h k l
28.131	2.9513	2 1 2
46.469	1.8752	4 2 2
53.510	1.6433	2 3 3

Average Lattice Constants = 11.3479

a= 9.7984 b= 8.2759 c =9.6138

$\alpha = \beta = \gamma = 90^O$

Density = 1.9117 $mg.cm^{-3}$

Crystal Form: Orthorhombic –A Center

Spacing Groups: Abm2 (39)

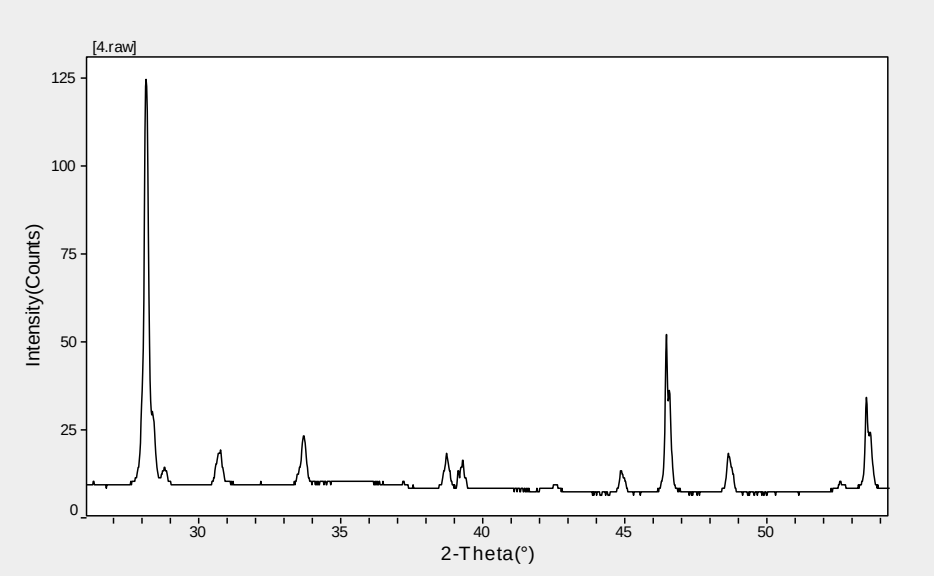

Figure (4.12) XRD spectrum of ($Ni_{0.5}S_{0.5}O_4$) sample

Table (4.10) Lattice Constants from Peak Locations and Miller Indices [Orthorhombic A-Center] of ($Ni_{0.3}S_{0.7}O_4$) sample

2Θ	d (nm)	h k l
28.131	2.8923	2 1 2
46.469	1.8377	4 2 2
53.510	1.6104	2 3 3

Average Lattice Constants = 11.3475

a= 9.7984 b= 8.2759 c =9.6138

$\alpha = \beta = \gamma = 90^O$

Density = 1.9138 $mg.cm^{-3}$

Crystal Form: Orthorhombic –A Center

Spacing Groups: Abm2 (39)

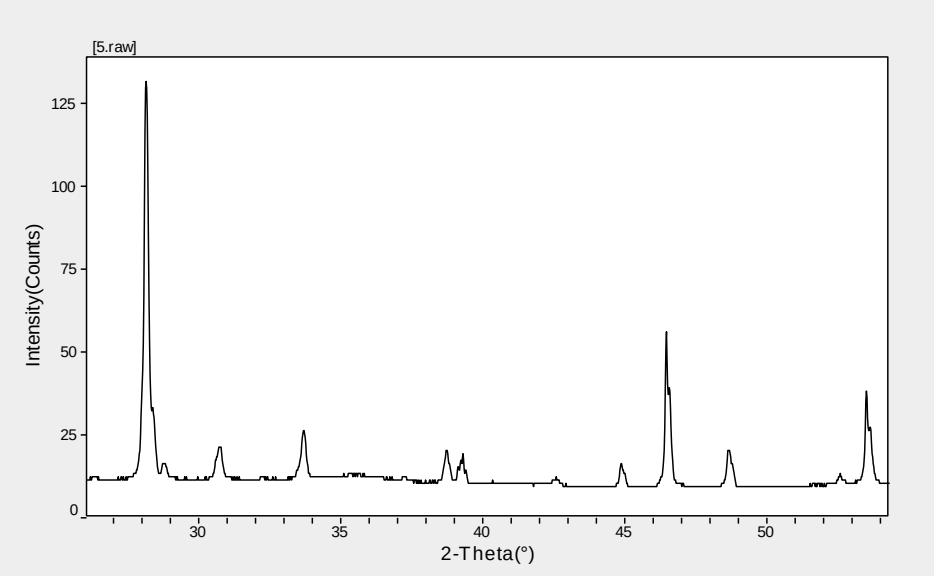

Figure (4.13) XRD spectrum of ($Ni_{0.3}S_{0.7}O_4$) sample

Table (4.11) Lattice Constants from Peak Locations and Miller Indices [Orthorhombic A-Center] of ($Ni_{0.1}S_{0.9}O_4$) sample

2Θ	d (nm)	h k l
28.131	2.8345	2 1 2
46.469	1.8009	4 2 2
53.510	1.5782	2 3 3

Average Lattice Constants = 11.3471

a= 9.7984 b= 8.2759 c =9.6138

$\alpha = \beta = \gamma = 90^O$

Density = 1.9144 $mg.cm^{-3}$

Crystal Form: Orthorhombic –A Center

Spacing Groups: Abm2 (39)

Table (4.12) some crystallite lattice parameter (c- form , a,b,c, β,α, γ, density ,Xs(nm) and d – spacing) of all samples that meade by ($Ni_xS_{x-1}O_4$)

Sample	a=b	c	α= β	γ	Density($g.cm^{-3}$)	d-spacing (A^o)
$Ni_{0.9}S_{0.1}O_4$	9.7984	9.6138	90	90	1.9013	2.26102
$Ni_{0.7}S_{0.3}O_4$	9.7984	9.6138	90	90	1.9035	2.47383
$Ni_{0.5}S_{0.5}O_4$	9.7984	9.6138	90	90	1.9117	2.26096
$Ni_{0.3}S_{0.7}O_4$	9.7984	9.6138	90	90	1.9138	2.21573
$Ni_{0.1}S_{0.9}O_4$	9.7984	9.6138	90	90	1.9144	2.17141

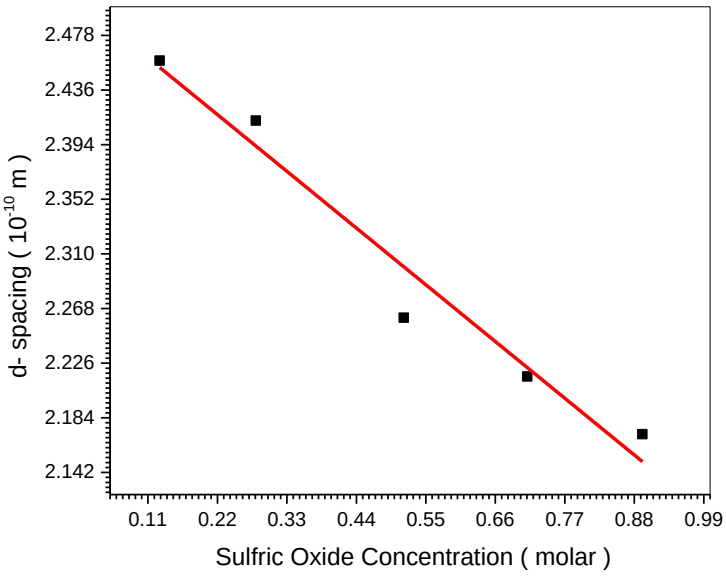

Figure (4.14) relationship between Nix rated and d-spacing of all (Ni 0.1 S 0.9 O4) samples

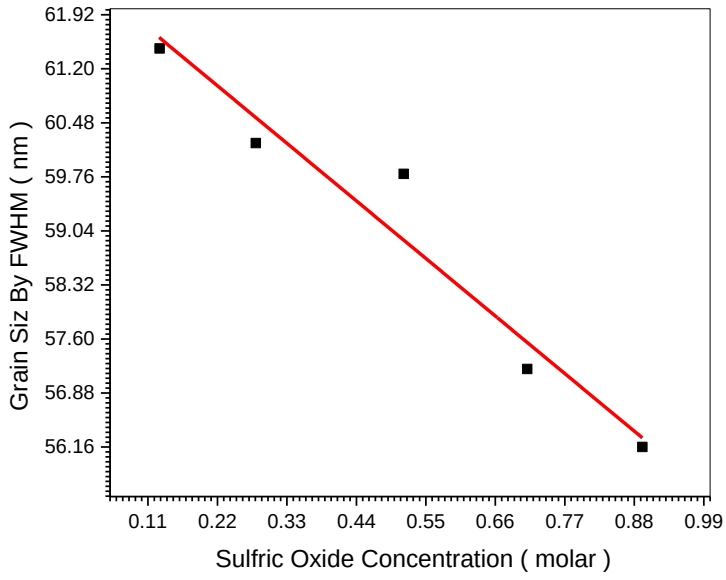

Figure (4.15) relationship between Nix rated and crystallite size of all (Ni 0.1 S 0.9 O4) samples

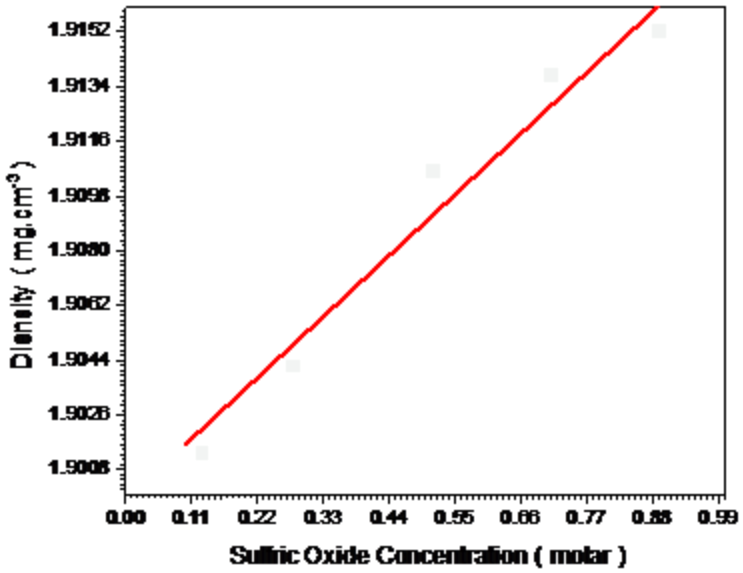

Figure (4.16) relationship between Nix rated and Density of all (Ni 0.1 S 0.9 O4) samples

(4.4)UV Result of ($Ni_x Al_{2(1-x)} O_4$)

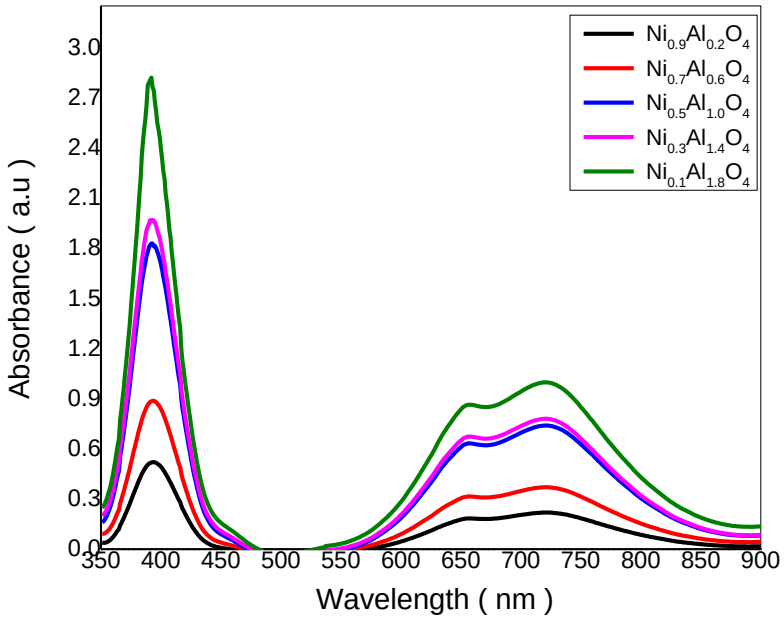

Figure (4.17) relation between absorbance and wavelengths of (Ni x Al2(1-x)O 4) samples

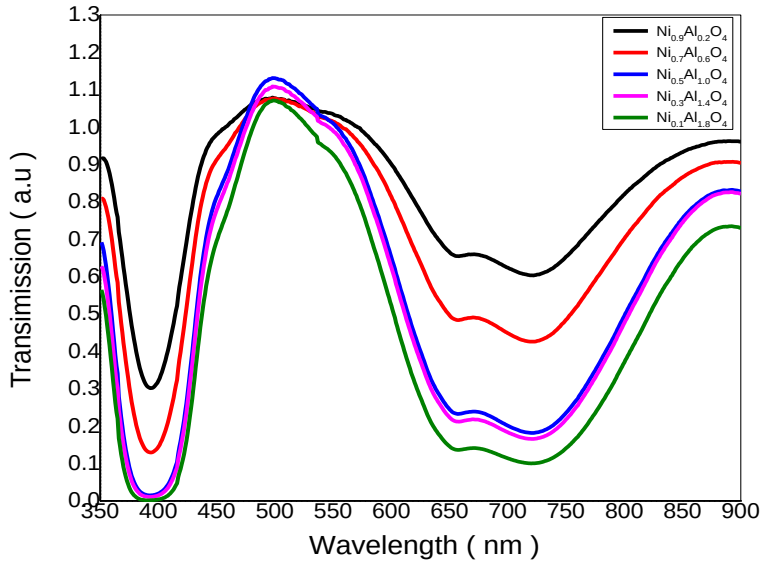

Figure (4.18) relation between transimission and wavelengths f (Ni x Al2(1-x)O 4) samples

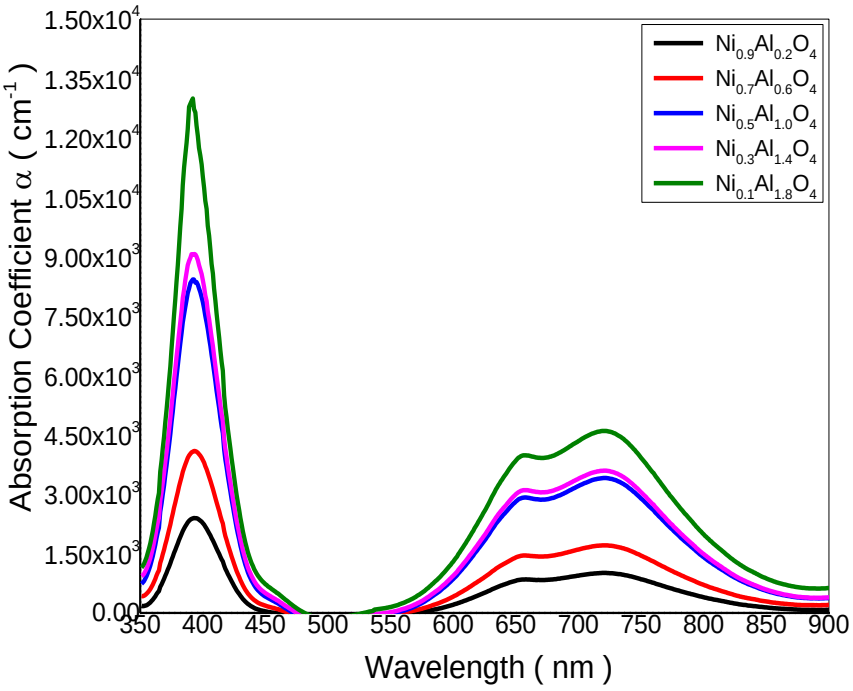

Figure (4.19) relation between absorption coefficient and wavelengths of (Ni x Al2(1-x)O 4) samples

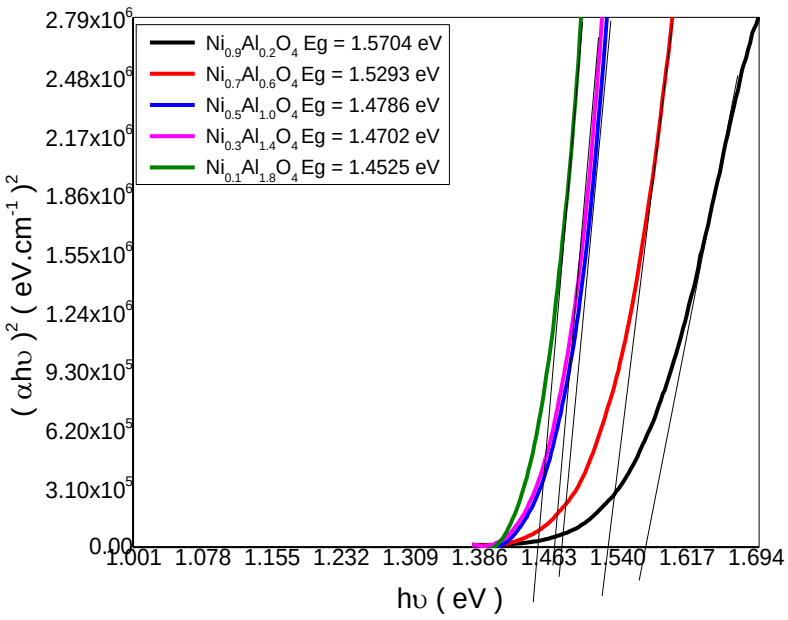

Figure (4.20) optical energy band gaups of (Ni x Al2(1-x)O 4) samples

(4.5) UV Results of ($Ni_xS_{1-x}O_4$)

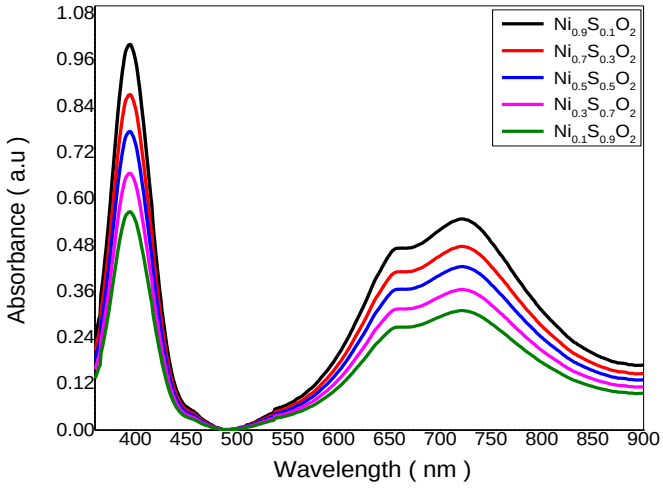

Figure (4.21) relation between absorbance and wavelengths of ($Ni_xS_{1-x}O_4$) samples

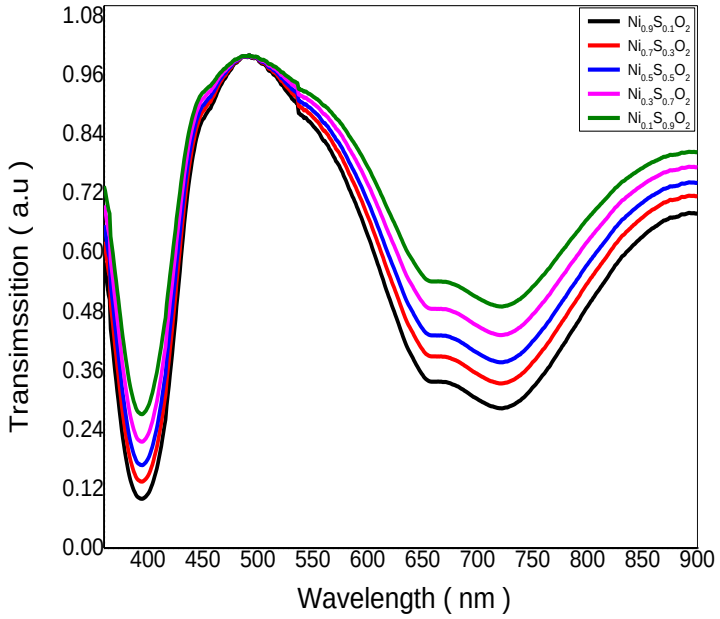

Figure (4.22) relation between transimission and wavelengths of (Ni x S 1-x O4) samples

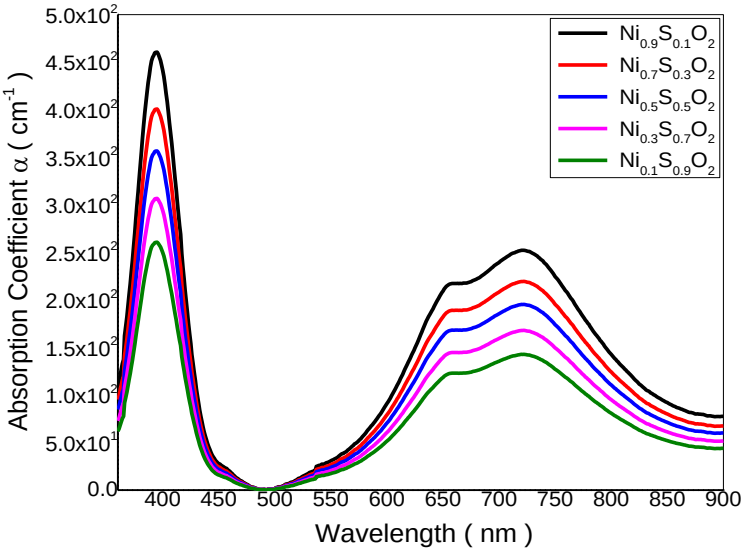

Figure (4.23) relation between absorption coefficient and wavelengths of (Ni x S 1-x O4) samples

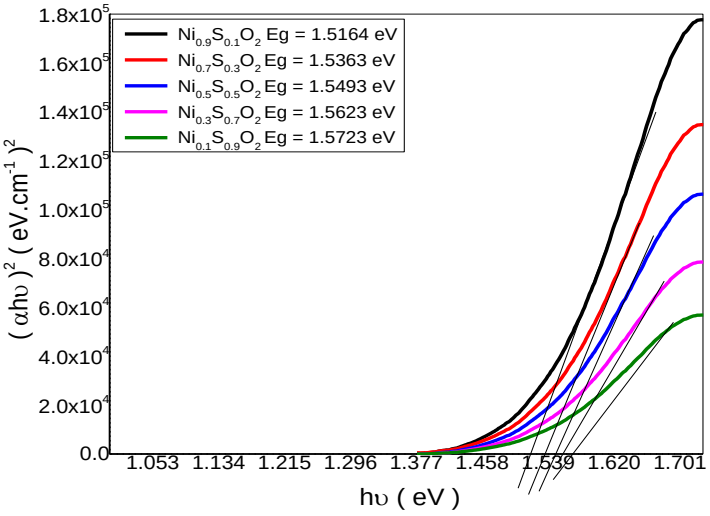

Figure (4.24) optical energy band gaups of ($Ni_x S_{1-x} O_4$) samples

(4.6) FTIR Results of ($Ni_xAl_{1-x} O_2$) samples

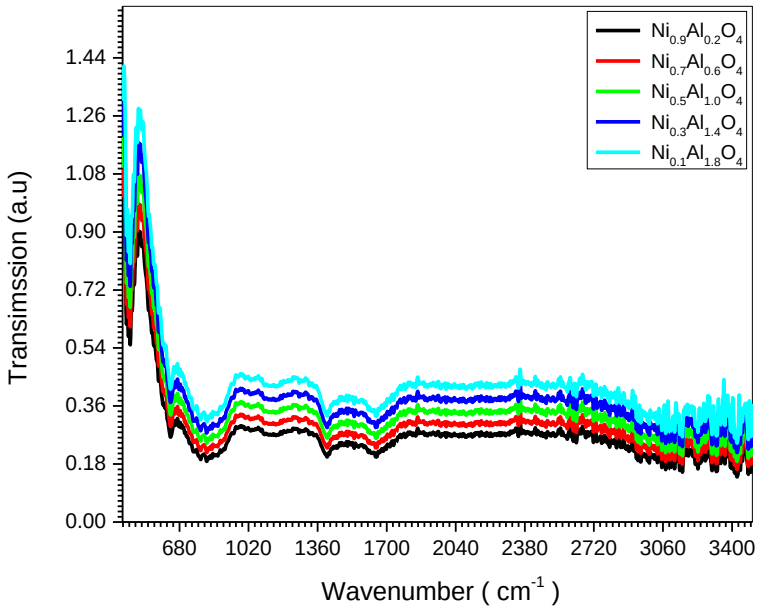

Figure (4.25) FTIR Results of ($Ni_xAl_{1-x} O_4$) samples

(4.7) FTIR Results of ($Ni_x S_{1-x} O_4$)samples

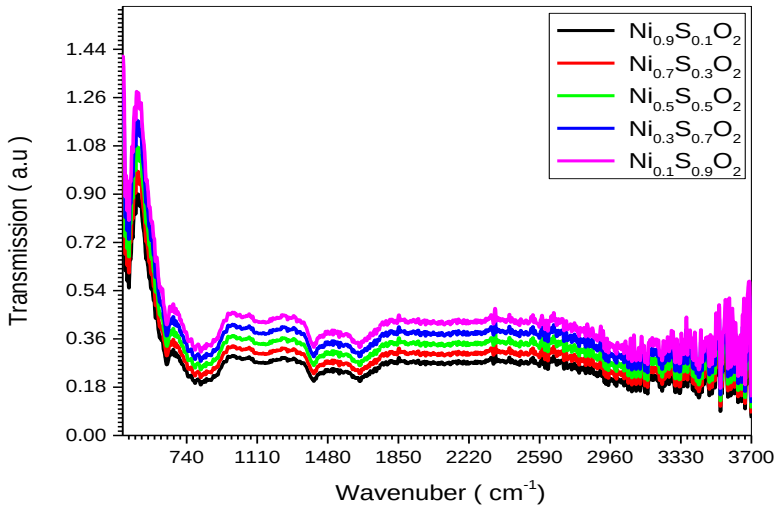

Figure (4.26) FTIR Results of (Ni xS 1-x O4) samples

Table(4-13) FTIR Parameters of ($Ni_x S_{1-x} O_4$)samples

No	Wavenumber (cm-1)	Vipration	FucationGrop
1	440	s-s stretch	Aryldisuilifdes
2	632	-c = c – H : C-H bend	
3	800	C-H bend	Aldehydes
4	1400	c – c stretch (in – ring)	aromatics
5	1650	N-H bend	I amines
6	2640	Vs (c – H)	B abs in diamond H in diamond Ib Diamond systhesized H indiamondIb B indiamond(type LL, two – phononregion)
7	3150	Vs (c – H)	H indiamondIb H indiamondIaA and Ib(near – colorless yellow, orange, brown, green, chameleon diamond)
8	3420	O-H stretching	Phenols & Alcohols
9	3540	V(o – H)	

(4.8) IV Solar Cells Results of ($Ni_x Al_{2(1-x)} O_4$)samples

Table(4.14) IV Solar Cells Results of ($Ni_{0.1}Al_{1.8}O_4$)samples

No	Voltage (V)	Current (mA)
1	0	7.52041
2	0.13874	7.5204
3	0.27888	7.52035
4	0.41902	7.52013
5	0.55916	7.51921
6	0.6993	7.51525
7	0.83944	7.49827
8	0.97958	7.42542
9	1.11972	7.11295
10	1.25986	5.77274
11	1.4	0

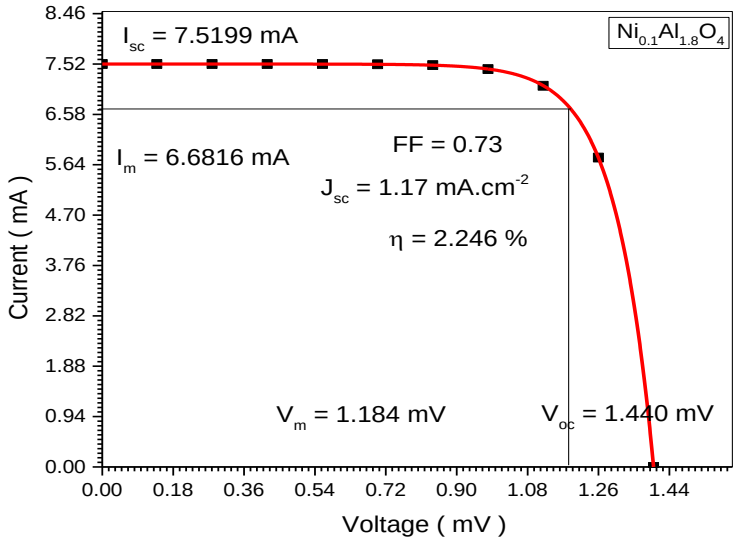

Figure (4.27) IV Solar Cells Results of ($Ni_{0.1}Al_{1.8}O_4$) samples

Table(4.15) Solar Cells Results of($Ni_{0.3}Al_{1.4}O_4$)samples

No	Voltage (V)	Current (mA)
1	0	6.69316
2	0.13874	6.69315
3	0.27888	6.69311
4	0.41902	6.69292
5	0.55916	6.69209
6	0.6993	6.68857
7	0.83944	6.67346
8	0.97958	6.60863
9	1.11972	6.33052
10	1.25986	5.13774
11	1.4	0

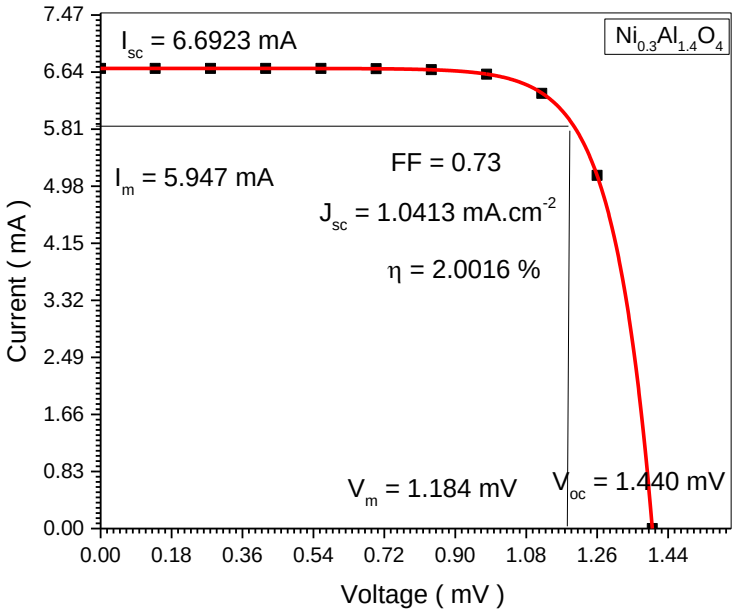

Figure (4.28) Results of ($Ni_{0.3}Al_{1.4}O_4$) samples

Table (4.16) Solar Cells Results of ($Ni_{0.5}Al_{0.1}O_4$) samples

No	Voltage (V)	Current (mA)
1	0	6.54275
2	0.13874	6.54274
3	0.27888	6.5427
4	0.41902	6.54251
5	0.55916	6.54171
6	0.6993	6.53827
7	0.83944	6.52349
8	0.97958	6.46012
9	1.11972	6.18826
10	1.25986	5.02229
11	1.4	0

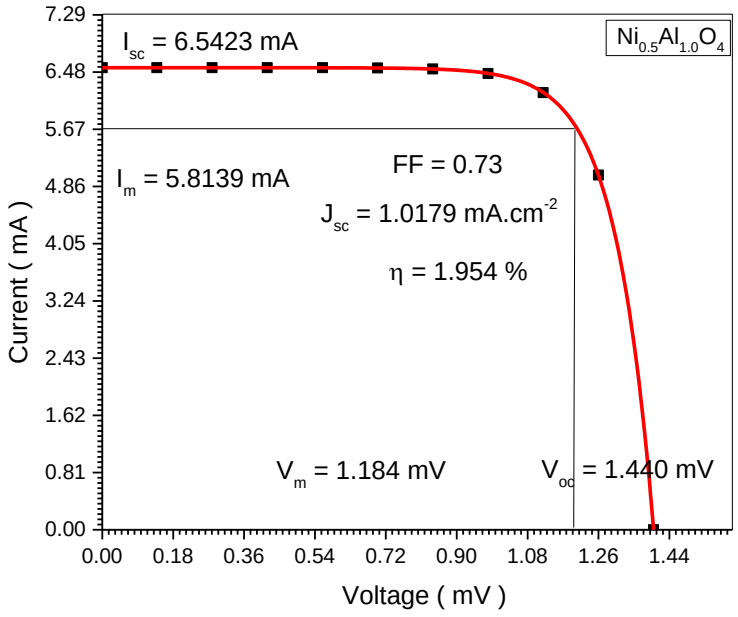

Figure (4.29) Solar Cells Results of (Ni 0.5Al0.1O4) samples

Table (4.17) Solar Cells Results of ($Ni_{0.7}Al_{0.6}O_4$) samples

No	Voltage (V)	Current (mA)
1	0	6.39235
2	0.13874	6.39234
3	0.27888	6.39229
4	0.41902	6.39211
5	0.55916	6.39133
6	0.6993	6.38796
7	0.83944	6.37353
8	0.97958	6.31161
9	1.11972	6.046
10	1.25986	4.90683
11	1.4	0

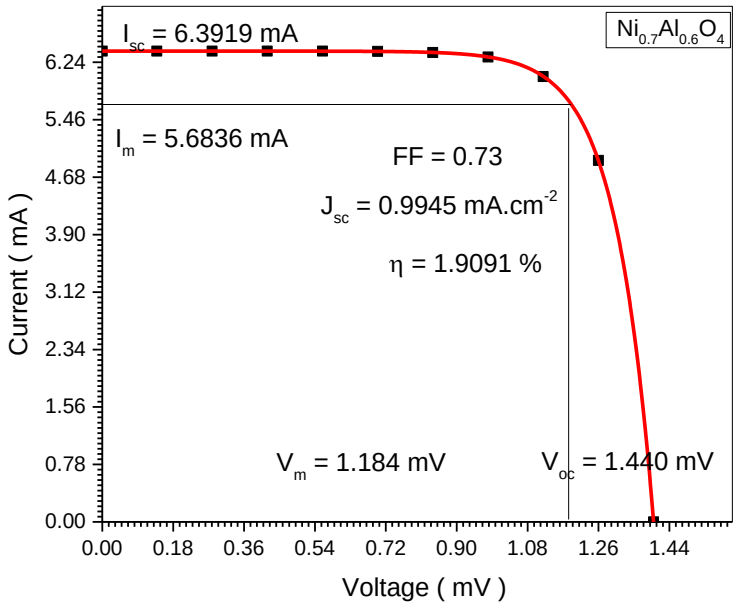

Figure (4.30) Solar Cells Results of (Ni 0.7Al0.6O4) samples

Table (4.18) Solar Cells Results of($Ni_{0.9}Al_{0.2}O_4$) samples

No	Voltage (V)	Current (mA)
1	0	6.24194
2	0.13874	6.24193
3	0.27888	6.24189
4	0.41902	6.24171
5	0.55916	6.24094
6	0.6993	6.23766
7	0.83944	6.22356
8	0.97958	6.1631
9	1.11972	5.90374
10	1.25986	4.79138
11	1.4	0

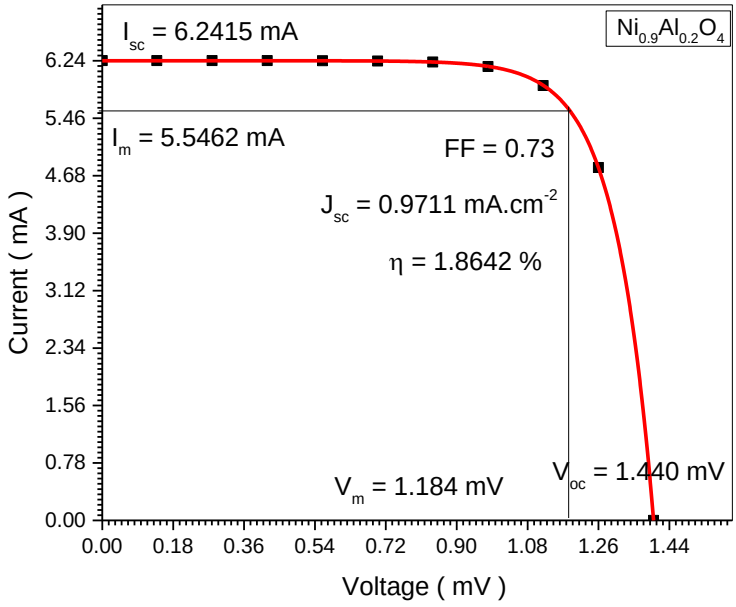

Figure (4.31) Solar Cells Results of (Ni 0.9Al0.2 O4) samples

(4.9)IV Solar Cells Results of ($Ni_xS_{1-x}O_4$) samples

Table (4.19) Solar Cells Results of ($Ni_{0.1}S_{0.9}O_4$) samples

No	Voltage (V)	Current (mA)
1	0	5.62808
2	0.13874	5.62807
3	0.27888	5.62803
4	0.41902	5.62787
5	0.55916	5.62718
6	0.6993	5.62422
7	0.83944	5.61151
8	0.97958	5.55699
9	1.11972	5.32314
10	1.25986	4.32017
11	1.4	0

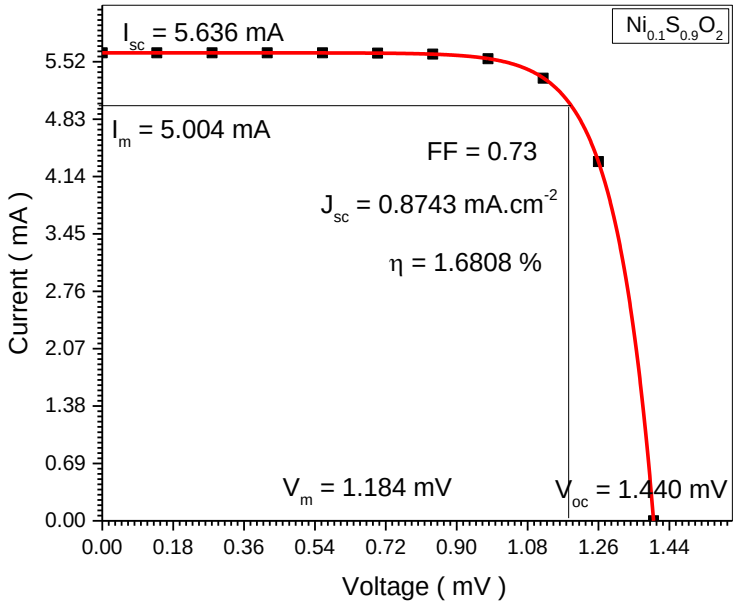

Figure (4.32) Solar Cells Results of (Ni0.1S0.9 O4) samples

Table (4.20) Solar Cells Results of ($Ni_{0.3}S_{0.7}O_4$) samples

No	Voltage (V)	Current (mA)
1	0	5.75746
2	0.13874	5.75745
3	0.27888	5.75741
4	0.41902	5.75725
5	0.55916	5.75654
6	0.6993	5.75351
7	0.83944	5.74051
8	0.97958	5.68474
9	1.11972	5.44551
10	1.25986	4.41948
11	1.4	0

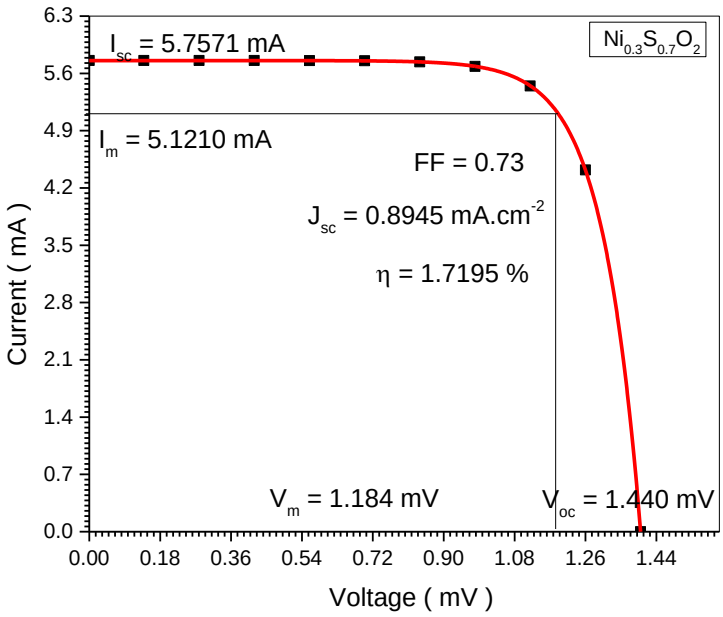

Figure (4.33) Solar Cells Results of (Ni 0.3S 0.7 O4) samples

Table (4.21) Solar Cells Results of ($Ni_{0.5}$ $S_{0.5}$ O4) samples

No	Voltage (V)	Current (mA)
1	0	5.88684
2	0.13874	5.88683
3	0.27888	5.88679
4	0.41902	5.88662
5	0.55916	5.8859
6	0.6993	5.8828
7	0.83944	5.86951
8	0.97958	5.81249
9	1.11972	5.56789
10	1.25986	4.5188
11	1.4	0

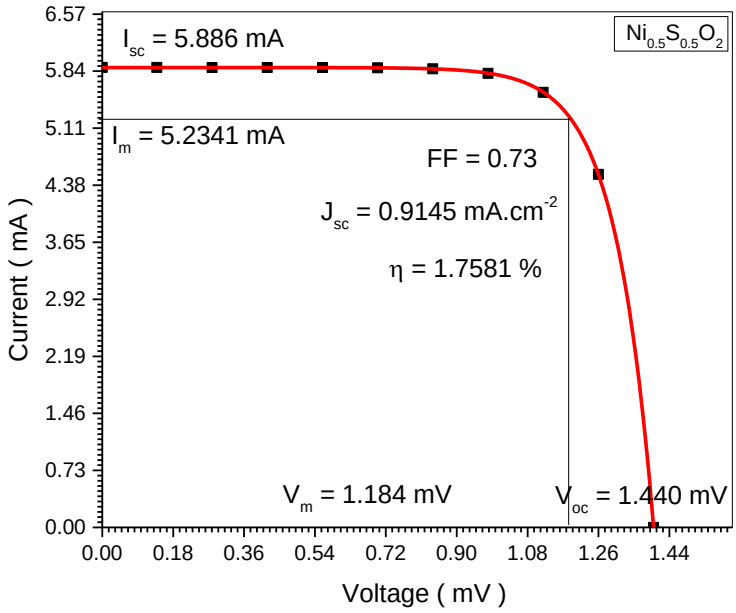

Figure (4.34) Solar Cells Results of (Ni0.5 S0.5 O4) samples

Table (4.22) Solar Cells Results of ($Ni_{0.7}$ $S_{0.3}$ O_4) samples

No	Voltage (V)	Current (mA)
1	0	6.01622
2	0.13874	6.01621
3	0.27888	6.01617
4	0.41902	6.016
5	0.55916	6.01526
6	0.6993	6.01209
7	0.83944	5.99851
8	0.97958	5.94024
9	1.11972	5.69026
10	1.25986	4.61811
11	1.4	0

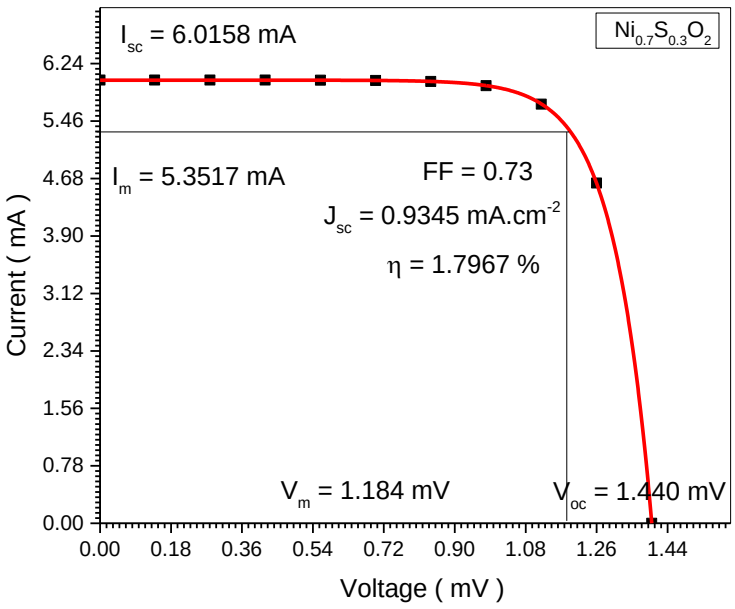

Figure (4.35) Solar Cells Results of (Ni0.7 S0.3 O4) samples

Table (4.23) Solar Cells Results of ($Ni_{0.9}S_{0.1}O_4$) samples

No	Voltage (V)	Current (mA)
1	0	6.46905
2	0.13874	6.46904
3	0.27888	6.469
4	0.41902	6.46882
5	0.55916	6.46802
6	0.6993	6.46462
7	0.83944	6.45001
8	0.97958	6.38735
9	1.11972	6.11856
10	1.25986	4.96571
11	1.4	0

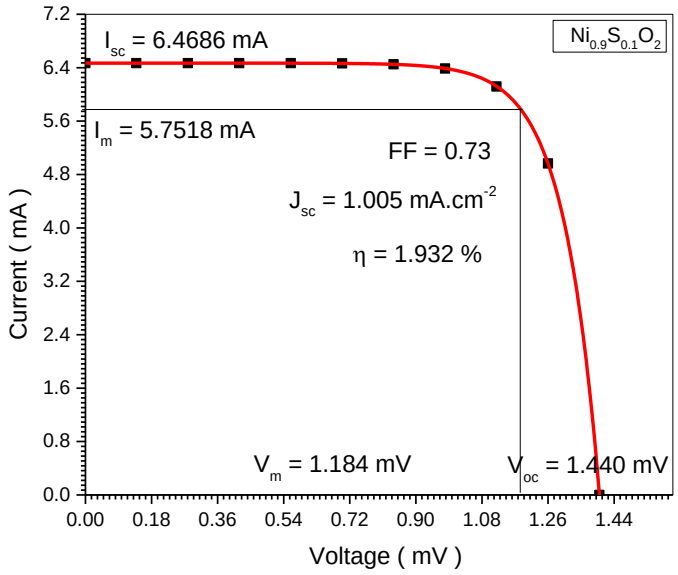

Figure (4.37) Solar Cells Results of (Ni 0.9S 0.1 O4) samples

Table (4.24) ($Ni_x Al_{2(1-x)} O_4$) samples

sample	I_{sc} (mA)	Im (mA)	Voc(V)	Vm(V)	Jsc(mA.cm-2)	FF	η%
$Ni_{0.1}Al_{1.8}O_4$	7.599	6.616	1.440	1.184	1.17	0.73	2.246
$Ni_{0.3}Al_{1.4}O_4$	6.6923	5.947	1.440	1.184	1.0413	0.73	2.0016
$Ni_{0.5}Al_{1.0}O_4$	6.5423	5.8139	1.440	1.184	1.0179	0.73	1.954
$Ni_{0.7}Al_{0.6}O_4$	6.3919	5.6836	1.440	1.184	0.9945	0.73	1.9091
$Ni_{0.9}Al_{0.2}O_4$	6.4215	5.5462	1.440	1.184	0.9711	0.73	0.8642

Table (4.25) ($Ni_x S_{1-x} O_4$) samples

sample	I_{sc} (mA)	Im (mA)	Voc(V)	Vm(V)	Jsc(mA.cm-2)	FF	η%
$Ni_{0.1}S_{0.9}O_4$	5.636	5.004	1.440	1.184	0.8743	0.73	1.6808
$Ni_{0.3}S_{0.7}O_4$	5.7571	5.1210	1.440	1.184	0.8945	0.73	1.7195
$Ni_{0.5}S_{0.5}O_4$	5.886	5.2341	1.440	1.184	0.9145	0.73	1.7581
$Ni_{0.7}S_{0.3}O_4$	6.0158	5.3517	1.440	1.184	0.9345	0.73	0.7967
$Ni_{0.9}S_{0.1}O_2$	6.4686	5.7518	1.440	1.184	1.005	0.73	1.932

4-10 **Discussion**

The optical and electric properties of the solar cell thin films $Ni_x\ AL_{2(1-x)}O_4$ and $Ni_xS_{1-x}O_4$ and their relation with the cell efficiency shows interesting result. For $Ni_x\ AL_{2(1-x)}O_4$, figures (4.7), (4.8) and (4.9), beside table (4.6) shows that as Ni molar concentration decreases and AL molar concentration increase the crystal spacing d, the Nano crystal size X_s and the matter density increase. According to figures (4.20),(4.21) and table (4.24), the absorption coefficient X and the cell efficiency decrease upon increasing the Ni concentration X, while causing the energy gap Eg to increase. This means that increasing the Nano crystal size the absorption coefficient and the solar efficiency increase while the energy gap decrease. The fact that increasing absorption coefficient and the decrease of energy gap increase the cell efficiency is consistent with common senle and theoretical models.

For $Ni_xS_{1-x}O_4$ figures (4.15),(4.16) and (4.17) beside table (4.12) shows that decreasing Ni concentration X and increasing S concentration decrease the d- spacing, Nano crystal size X_s while it increase the density. Figures (4.20),(4.21) for the absorption coefficient X and energy gap Eg, beside table (4.25) for the cell efficiency shows that upon increasing the Ni concentration X the absorption coefficient and the efficiency increase, while the energy gap decrease. This result conform also with the well-known physical the arise. This means that increasing the Nano size increases the absorption coefficient and the efficiency but causing the energy gap to decrease.

4-11 Conclusions

Increasing Ni concentration for the thin film $Ni_x\ AL_{2(1-x)}O_4$ increase the energy gap while the non-crystal size, crystal spacing, mass density, absorption coefficient and solar cell efficiency decease. For the thin film $Ni_xS_{1-x}O_4$, that increase of Ni concentration increase crystal spacing Nano crystal size absorption coefficient and cell efficiency, but causes the energy gap and density to decrease.

4-12 Future work

- The thermal and mechanical properties of the samples can be also studied.
- The electrical and optical properties of new elements other than Ni, AL and S can be examined.
- The result obtained can be applied to design new solar cells and light sensors.

References

[1]- Design and feasibility study of PV systems in Kenya. Kenya: JSB.

[2]- Design and feasibility study of PV systems in Kenyaoufang lin l2010

[3]-April lv bin‹2009 [4]- R. L. David, Handbook of Chemistry and Physics, 87th ed., CRC Press (1998)

[5]- M.A. Rahman, A review on semiconductors including applications and temperature effects in semiconductors, Am. Sci. Res. J. Eng., Technol., Sci. 7 (2014) 50-70.

[6] - H.L. Tan, F.F. Abdi, Y.H. Ng, Heterogeneous photocatalysts: an overview of classic and modern approaches for optical, electronic, and charge dynamics evaluation, Chem. Soc. Rev.48 (2019) 1255-1271

[7] - L. Smart, E. Moore, Solid state chemistry - An introduction, 2nd Ed., Chapman & Hall,London, 1996.

[8] - L. Smart, E. Moore, Solid state chemistry - An introduction, 2nd Ed., Chapman & Hall,London, 1996.

[9] - J.P. Bird, Encyclopedia of materials: Science and technology, Semiconductors: An introduction, Elsevier, 2002.

[10]- G. Naudin, T. Entradas, B. Barrocas, O.C. Monteiro, Titanate nanorods modified with nanocrystalline ZnS particles and their photocatalytic activity on pollutant removal, J. Mater.Sci. Technol. 32 (2016) 1122-1128.

[11]- Y. Ma, X. Wang, Y. Jia, X. Chen, H. Han, C. Li, Titanium dioxide-based nanomaterials for photocatalytic, Chem. Rev. 114 (2014) 9987-10043.

[12] - A.B. Djurišić, Y.H. Leung, A.M.C. Ng, Strategies for improving the efficiency of semiconductor metal oxide photocatalysis, Mater. Horiz. 1 (2014) 400-410.

[13] - A.B. Djurišić, Y.H. Leung, A.M.C. Ng, Strategies for improving the efficiency of semiconductor metal oxide photocatalysis, Mater. Horiz. 1 (2014) 400-410

[14] - M.K. Nowotny, P. Bogdanoff, T. Dittrich, S. Fiechter, A. Fujishima, H. Tributsch,Observations of p-type semiconductivity in titanium dioxide at room temperature, Mater. Lett.64 (2010) 928-930.

[15] - P.A. Korzhavyi, B. Johansson, Literature review on the properties of cuprous oxide Cu2O and the process of copper oxidation, Svensk Kärnbränslehantering AB, Stockholm, 2011.

[16] - C.L. Wong, Y.N. Tan, A.R. Mohamed, A review on the formation of titania nanotube photocatalysts by hydrothermal treatment, J. Environ. Manage. 92 (2011) 1669-1680.

[17] - S. Zhao, J. Li, L. Wang, X. Wang, Degradation of rhodamine B and safranin-T by MoO3:CeO2 nanofibers and air using a continuous mode, Clean: Soil, Air, Water 38 (2010)268-274

[18] - Y.H. Yin, Z.P. Wu, M. Zhao, G. Wu, Y.S. Li, Z.X. Guo, W.J. Yu, L.S. Tang, Preparationof highly dispersed WO3 nanoparticles on carbon nanotubes and application as visible photocatalyst, J. Nanosci. Nanotechnol. 19 (2019) 4771-4777.

[19]- B. Barrocas, T.J. Entradas, C.D. Nunes, O.C. Monteiro, Titanate nanofibers sensitized with ZnS and Ag2S nanoparticles as novel photocatalysts for phenol removal, Appl. Catal. B 218(2017) 709-720.

[20]- D.V. Bavykin, J.M. Friedrich, F.C. Walsh, Protonated titanates and TiO2 nanostructured materials: Synthesis, properties, and applications, Adv. Mater. 18 (2006) 2807-2824.

[21]- T.J. Entradas, J.F. Cabrita, B. Barrocas, M.R. Nunes, A.J. Silvestre, O.C. Monteiro,Synthesis of titanate nanofibers co-sensitized with ZnS and Bi2S3 nanocrystallites and their application on pollutants removal, Mater. Res. Bull. 72 (2015) 20-28.

[22]- B. Barrocas, S. Sério, A. Rovisco, M.E. Melo Jorge, Visible-light photocatalysis in a0.6Ho0.4MnO3 films deposited by RF-magnetron sputtering using nanosized powder compacted target, J. Phys. Chem. C 118 (2014) 590-597.

[23]- S. Feizpoor, A. Habibi-Yangjeh, S. Vadivel, Novel TiO2/Ag2CrO4 nanocomposites: Efficient visible-light-driven photocatalysts with n-n heterojunctions, J. Photochem. Photobiol.A Chem. 341 (2017) 57-68.

[24]- M. Shekofteh-Gohari, A. Habibi-Yangjeh, Fe3O4/ZnO/CoWO4 nanocomposites: Novel magnetically separable visible-light-driven photocatalysts with enhanced activity in degradation of different dye pollutants, Ceram. Inte. 43 (2017) 3063-3071.

[25]- O. Akhavan, R. Azimirad, Photocatalytic property of Fe2O3 nanograin chains coated byTiO2 nanolayer in visible light irradiation, Appl.., A 369 (2009) 77-82.

[26]prof.mubarakdirrar

[27]- Wooten, F. Optical Properties of Solids. New York: Academic.1972.

[28]- Woggon, U. Optical Properties of Semiconductor Quantum Dots. Berlin: Springer. 1996

[29]- M. Born and E. Wolf, “Principles of Optics,” Pergamon Press, United Kingdom, 6th ed. 1993

[30]- Linda J. Vandergriff Director of Photonics System Engineering Science Applications International Corporation McLean, Virginia, 2008.

[31]- A.Lipson, S.G.Lipson,H.Lipson,"Optical Physics ", Cambridge University Press, fourth edition (2011). [37]- O. Stenzel," The Physics of Thin Film Optical Spectra–an introduction ", Springer,Germany, (2005).

[32]- J.A., Ed. McGraw Lange’s Handbook of Chemistry,-Hill, Inc., New York. (1992).

[33]- Weast, R.C., Ed.. Handbook of Chemistry and Physics, 56th Edition, CRC Press, Cleveland. 14th Edition, (1975).

[34]-D. A. Neamen," Semiconductor Physics and Devices ", University of New Mexico ,(1992)

[35]-R. Ellingson and M. Heben, Absorption coefficients of semiconductor thin films, University of Toledo, October 2013

[36]- Charles Ktile introduction to Solid State Physics 8th addition John Wiley & Sons, Inc(2005)ISBN 0-471-41526-x.

[37]- Harland G. Tompkins and James N. Hilfiker, Spectroscopic Ellipsometry, Momentum press (2015).

[38]- Sirotin and M.Shaskolskays, “Fundamental of Crystal Physics” ,Mir Publishers, Moscow, (1982). [45]- Baumeister PW, Optical absorption of cuprous oxide, Physical Review,1961.

[39]- K. L. Chopra, "Thin Film Devices Application", Plenum Press,New York, (1983).

[40]- N.A. Subrahamanyam, "Textbook of Optics", 9edition, 1TDelhi1TIndia, (1977).

[41]- H.S. Nalwa, Handbook of Thin Films Materials, Academic Press All rights of reproduction in any form reserved, 2001

[42]- Dikshitulu K. Kalluri, principle of electromagnetic waves and materials, 2ndedition,CRC Press, Taylor and Francis group,2018, ISBN 13: 4978-1-3329-8.

[43]- E.Y.Tsymbal, Optical properties of solids, academic press New York and London, 1972.

[44]- L. Solymar, D. Walshr R. R. A. Syms, electrical properties of materials, Ninth edition Oxford University Press, 2014, ISBN 978–0–19–870278–8.

[45]- M. K. Jayaraj, optical and electrical properties, material Horizons; from nature to nanomaterial, 1st edition 2020, ISBN. 10-98115333x.

[46]- Michael B. Heaney. "Electrical Conductivity and Resistivity."Copyright CRC Press LLC. 2000.

[47]-Gonzale, W and Mancini, H.L, an introduction to materials science. Princeton university press (2004). ISBN 9780-691-07097-1

[48]- Uichiro.M introduction to electron theory, Cambridge university press, 1st edition 2001 ISBN-10 0521587099.

[49]- synthesizing SnO2 quantam dots, Nanotechnology 17, 2386-2389 (2006).

[50]- J. Xu, H. Yang, Q. Yu, L. Chang, X. Pang, X. Li, H. Zhu., M. Li and G. Zou,

[51]- Synthesis and characterization of hollow microspheres coated by SnO2 nanoparticles,

[52]- Mater. Lett. 61, 1424-1428 (2007).

[53]- J. Zhang and L. Gao, Synthesis and characterization of antimony doped tin oxide

[54]- (ATO) nanoparticles by a new hydrothermal method, Mater. Chem. Phys. 87, 10-13

[55]- C. Xu, J. Tamaki, N. Miura and N. Yamazoe, Grain size effects on gas sensitivity of

[56]- porous SnO2 based elements, Sens. Actuators B 3, 147-155 (1991).

[57]- H. Zhu, D. Yang, G. Yu, H. Zhang and K.Yao, A simple hydrothermal route for

[58]- synthesizing SnO2 quantam dots, Nanotechnology 17, 2386-2389 (2006).

[59]- J. Xu, H. Yang, Q. Yu, L. Chang, X. Pang, X. Li, H. Zhu., M. Li and G. Zou

[60]- Synthesis and characterization of hollow microspheres coated by SnO2 nanoparticles,

[61]- Mater. Lett. 61, 1424-1428 (2007).

[62]- J. Zhang and L. Gao, Synthesis and characterization of antimony doped tin oxide

[63]- B. F. Fei, H. Yun, H. Ping, T. Y. Wen and J. Z Jie, One-step synthesis of mono

[64]- dispersed antimony-doped tin oxide suspension, Mater. Letters 60, 3126-3129 (2006).

[65]- of Sb-doped SnO2 nanoparticles used as transparent conductive films, Mater. Res.

[66]- nanocrystallites, Mater. Res. Bull. 37, 2453-2458 (2002).

[67] temperature combustion synthesis, J. Chinese Ceram. Soc. 28, 534-537 (2000).

[68]- F. Gu, S. F. Wang, M. K. Lü, G. J. Zhou, D. Xu and D. R. Yuan, Photo- luminescence

[69]- properties of SnO2 nanoparticles synthesized by sol–gel method, J. Phys. Chem. B

[70]- 108, 8119-8125 (2004).

[71]- J. Q. Hu, Y. Bando and D. Golberg, Self-catalyst growth and optical properties of

[72]- novel SnO2 fishbone-like nanoribbons, Chem. Phys. Lett. 372, 758-762 (2003).

[73]- H. Zhu, D. Yang, G. Yu, H. Zhang and K.Yao, A simple hydrothermal route for

[74]- synthesizing SnO2 quantam dots, Nanotechnology 17, 2386-2389 (2006).
[75]- J. Xu, H. Yang, Q. Yu, L. Chang, X. Pang, X. Li, H. Zhu., M. Li and G. Zou
[76]- Synthesis and characterization of hollow microspheres coated by SnO2 nanoparticles
[77]- Mater. Lett. 61, 1424-1428 (2007).
[78]- J. Zhang and L. Gao, Synthesis and characterization of antimony doped tin oxide
[79]-(ATO) nanoparticles by a new hydrothermal method, Mater. Chem. Phys. 87, 10-13
[80]-(In2019) Ganga R. Neupanea, AmritKaphlea, ParameswarHaria,b,*
[81](In2020) SeyedehLalehMousavia, FaridJamali-Sheinib,□, Mohammad Sabaeianc,d, RaminYousefie
[82]-(nI2020) Gurleen Kaur a,b,*, Zheng Xin b, RanjaniSridharan b, Aaron Danner a,b, Rolf Stangl b
[83]-(In 2016) P. Mandal n, S. Sharma
[84]-(In 2020) Hongen Li , Yizhi Hu , Yue Yang *, Yonggang Zhu
[85]- (in 24-8-2017)Diego Cortes-Arriagada, Nery Villegas-Escobar, ´ Daniela E. Ortega
[86]- ((In JANUARY 2013) P. H. Lu, K. Wang, Z. Lu, A. J. Lennon, and S. R. Wenham, Member, IEEE
[87]- (In 2018) Tong Chen a, Yunfei Shang a, ShuweiHao a, b, *, Li Tian a, YuedanHou a, Chunhui Yang a
[88]-(In 2018) T. Thirugnanasambandan a, K. Pal b,*, Sidhu A. c, M. AbdElkodous d, H. Prasath e,
K. Kulasekarapandian f, A. Ayeshamariam g, J. Jeevanandam h
[89]- "aluminum nitrate" (http://chemister.ru/Database/properties-en.php?dbid=1&id=8810) .
[90]- . NIOSH Pocket Guide to Chemical Hazards. "#0024"
(https://www.cdc.gov/niosh/npg/npgd0024.ht
[91]- Pradyot Patnaik. Handbook of Inorganic Chemicals. McGraw-Hill, 2002, ISBN 0-07-049439-8
[92]- Perry's Chem Eng Handbook, 7th Ed
[93]- Lascelles, Keith; Morgan, Lindsay G.; Nicholls, David; Beyersmann, Detmar (2005). "Nickel

[94]- Morosin, B.; Haseda, T. (1979). "Crystal Structure of the β Form of Ni(NO3)2.4H2O". Acta Crystallographica Section B: Structural Crystallography and Crystal Chemistry. 35 (12): 2856–2858.

[95]- Gallezot, P.; Weigel, D.; Prettre, M. (1967). "Structure du Nitrate de Nickel Tétrahydraté". Acta Crystallographica

[96]- Charles Ktile introduction to Solid State Physics 8th addition John Wiley & Sons, Inc(2005)ISBN 0-471-41526-x.

[97] Infrared Spectroscopy: Fundamentals and Applications B. Stuart,John Wiley & Sons, Ltd 2004, ISBNs: 0-470-85427-8.

[98] L.H Omari and H. Lassri, Structural and optical properties of Fe-doped ruddlesden – popper Ca3 Ti2-xFex O7-δ nanoparticles Elsevier B. V. 2020.

[99]- Perkampus, Heinz-Helmut, UV-VIS Spectroscopy and Applications, Springer Lab Manuals,1992 Ujjwal, A K Sen, UV-VIS Spectroscopy: absorption Spectroscopy, Lab Lambert Academic.